THE JOURNAL OF BIOLOGICAL CHEMISTRY VOL. 291, NO. 9, pp. 4308–4322, February 26, 2016

Deletion of *Mbtps1* (*Pcsk8*, *S1p*, *Ski-1*) Gene in Osteocytes Stimulates Soleus Muscle Regeneration and Increased Size and Contractile Force with Age*

Received for publication, August 18, 2015, and in revised form, December 22, 2015 Published, JBC Papers in Press, December 30, 2015, DOI 10.1074/jbc.M115.686626

Jeff P. Gorski[‡1], Nichole T. Huffman[‡], Julian Vallejo[§], Leticia Brotto[§2], Sridar V. Chittur[¶], Anne Breggia[‖], Amber Stern[‡‡], Jian Huang[§2], Chenglin Mo[§2], Nabil G. Seidah[§§], Lynda Bonewald[‡], and Marco Brotto[§2]**

From the [‡]Department of Oral and Craniofacial Sciences, University of Missouri-Kansas City Center of Excellence in the Study of Dental and Musculoskeletal Tissues, School of Dentistry, [§]Muscle Biology Research Group, School of Nursing and Health Studies, and [**]School of Computing and Engineering, University of Missouri-Kansas City, Kansas City, Missouri 64108, [¶]Center for Functional Genomics, University at Albany, Rensselaer, New York 12144, [‖]Maine Medical Center, Portland, Maine 04102, [‡‡]Engineering Systems, Inc., Charlotte, North Carolina 28277, and [§§]Institut de Recherches Cliniques Montreal, Montreal, Quebec H2W IR7, Canada

Conditional deletion of *Mbtps1* (cKO) protease in bone osteocytes leads to an age-related increase in mass (12%) and in contractile force (30%) in adult slow twitch soleus muscles (SOL) with no effect on fast twitch extensor digitorum longus muscles. Surprisingly, bone from 10–12-month-old cKO animals was indistinguishable from controls in size, density, and morphology except for a 25% increase in stiffness. cKO SOL exhibited increased expression of *Pax7*, *Myog*, *Myod1*, *Notch*, and *Myh3* and 6-fold more centralized nuclei, characteristics of postnatal regenerating muscle, but only in type I myosin heavy chain-expressing cells. Increased expression of gene pathways mediating EGF receptor signaling, circadian exercise, striated muscle contraction, and lipid and carbohydrate oxidative metabolism were also observed in cKO SOL. This muscle phenotype was not observed in 3-month-old mice. Although *Mbtps1* mRNA and protein expression was reduced in cKO bone osteocytes, no differences in *Mbtps1* or *cre* recombinase expression were observed in cKO SOL, explaining this age-related phenotype. Understanding bone-muscle cross-talk may provide a fresh and novel approach to prevention and treatment of age-related muscle loss.

Bone osteocytes are multifunctional endocrine cells. Osteoid osteocytes control bone mineralization by secretion of DMP1, phosphate-regulating endopeptidase homolog, *X*-linked (PHEX), and matrix extracellular phosphoglycoprotein (MEPE) (1), whereas mature osteocytes secrete sclerostin, an inhibitor of bone formation, and regulate phosphate homeostasis and, indirectly, bone mineralization via production of FGF23 (2). Osteocytes are the mechanosensory cells in bone and appear to regulate muscle function and myogenesis (3–5). Specifically, deletion of connexin43 in osteoblasts/osteocytes shows it is involved in postnatal bone-muscle cross-talk via an osteocalcin-mediated stimulation of muscle formation and function (5). Differentiated muscle cells, in return, secrete as yet unidentified factors that protect osteocytes against apoptosis and produce a factor that synergizes with fluid flow shear stress to increase prostaglandin E_2 production by osteocytes (6). Myogenesis in adult muscle occurs via activation of satellite (stem) cells during muscle regeneration after injury or exercise-induced damage (7, 8). Distinct populations of satellite cells appear to be responsible for regeneration of fast twitch and slow twitch myofibers (9, 10), respectively.

MBTPS1 (SKI-1, PCSK8, S1P)[3] is the eighth member of the proprotein convertase family of proteases (11). Localized to the cis/medial Golgi, MBTPS1 catalyzes the mandatory first cleavage of transmembrane-bound transcription factors like SREBP1 and cAMP-response element-binding protein; once released, their DNA binding domains are imported into the nucleus where they regulate transcription (12). Interestingly, MBTPS1 is required for the transcription of a number of bone matrix and mineralization-related genes including type XI collagen, *Phex*, *Dmp1*, fibronectin, and fibrillin in bone osteoblasts and osteocytes. Correspondingly, inactivation of MBTPS1 by AEBSF or specific inhibitor decanoyl-Arg-Arg-Leu-Leu-chloromethyl ketone blocks transcription of the aforementioned genes and inhibits mineralization (13, 14). These results demonstrated that the differentiated phenotype of osteoblastic cells and possibly osteocytes depends upon MBTPS1.

Having identified a functional role for MBTPS1 in osteoblasts and osteocytes *in vitro*, we asked whether skeletal functions require MBTPS1 *in vivo*. Because deletion of *Mbtps1* in

* This work was supported by National Institutes of Health Grants AR052775 (to J. P. G.), P01 AG039355 (to L. B. and M. B.), and RC2 AR058962 (to L. B. and M. B.); Canada Research Chair 216684 (to N. G. S.); and a University of Missouri Research Board bridging grant (to J. P. G.). The authors have no conflict of interest to disclose regarding the work presented in this manuscript. The content is solely the responsibility of the authors and does not necessarily represent the official views of the National Institutes of Health.
The data discussed in this publication have been deposited in NCBI's Gene Expression Omnibus and are accessible through GEO Series accession numbers GSE69975 and GSE69985.
[1] To whom correspondence should be addressed. Tel.: 816-235-2537; Fax: 816-235-5524; E-mail: gorskij@umkc.edu.
[2] Present address: Bone-Muscle Collaborative Sciences, College of Nursing and Health Innovation, University of Texas, Arlington, TX 76019.

[3] The abbreviations used are: MBTPS1, membrane-bound transcription factor peptidase 1; SKI-1, subtilisin kexin-like protease 1; S1P, site 1 protease; PCSK8, proprotein convertase subtilisin kexin 8; SOL, soleus muscle; EDL, extensor digitorum longus muscle; young, 3-month-old; adult, 10–12-month-old; cKO, conditional deletion of *Mbtps1*; AEBSF, 4-(2-aminoethyl)-benzenesulfonyl fluoride; CT, computed tomography; Mg29, mitsugumin 29; MYOG, myogenin; Ct, cycle threshold.

mice is embryonically lethal, we initially chose to use the late osteoblast/embedding osteocyte-restricted *Dmp1-cre* (15) and the *3.6 Col1-cre* (16), which is expressed in long bones and skull in addition to skin and tendon. We showed that *3.6 Col1-cre Mbtps1* cKO mice are born with a caudal regression-like spinal phenotype (17). In contrast, analysis of 3-month-old (young) and 10–12-month-old (adult) *Dmp1-cre Mbtps1* cKO mice revealed that MBTPS1 acts as a repressor of muscle myogenesis only in adults because its deletion in bone increases the size, contractile force, and regeneration of soleus muscles with age.

Experimental Procedures

Production of Dmp1-cre Mbtps1 cKO Mice—Animals were maintained in the University of Missouri-Kansas City Laboratory Animal Research Center under an approved protocol; this is an Association for Assessment and Accreditation of Laboratory Animal Care-accredited facility. *Mbtps1*-floxed mice were obtained from Dr. Jay Horton, Southwest Medical School and Dr. Linda Sandell, Washington University (18, 19); *Dmp1-cre* mice were obtained from Dr. Lynda Bonewald, University of Missouri-Kansas City (15). Males (*Mbtps1*(flx/+):*Dmp1*(*cre*/+)) were crossed with females (*Mbtps1*(flx/flx)) to obtain $Mbtps1^{cKO}$ mice (*Mbtps1*(flx/flx):*Dmp1*(*cre*/+)) offspring; this strategy deletes exon 2 of the *Mbtps1* gene and should be effective in ablating expression of all expressed forms containing the catalytic site (18). Only male *Mbtps1* cKO (*Mbtps1*(flx/flx) × *Dmp1-cre*(+/−)) and control mice (*Mbtps1*(flx/flx)) were used here to limit the study size and the effects of the estrous cycle. Unless otherwise noted, mice were maintained on standard mouse chow with free access to food and water and housed in ventilated cages with filter bonnets in rooms with a regulated 12-h light and 12-h dark cycle. Offspring were found to be viable throughout the pregnancy and postnatal period. Phenotypic characteristics for P10, 12-week-old, and 40-week-old mice were based on observations of *Mbtps1* cKO mice along with a comparable number of control littermates.

Genotyping—Mice were genotyped using DNA isolated from tail segments obtained at weaning. Tail segments were digested in 10 mM Tris-HCl, pH 8.0, containing 25 mM EDTA, 0.5% SDS, 50 mM NaCl, and 0.5 mg/ml proteinase K. A saturated solution of sodium chloride was then added to the digests to precipitate residual contaminating protein. Extracts were centrifuged for 25 min at room temperature, and the DNA-containing supernatant was precipitated using 80% isopropanol. Resulting pellets were then washed with 70% ethanol and allowed to air-dry. Dried pellets were hydrated with 0.01 M Tris-HCl buffer, pH 8.0, containing 1 mM EDTA, and the DNA concentration was determined by UV spectrophotometry.

DNA samples were genotyped using PCR with gene-specific primers for *Mbtps1* (18), *Dmp1-cre* (15), and *Jarid1/2* (20), a marker of sex. Primers used were as follows: for *Mbtps1*: P1, 5′-GAGAGCTGCAGATGACAGGGGACACAG-3′ and P2, 5′-GCCCAATCCACCGCTCTGTAGCGGAC-3′ (floxed product = 434 bp, wild type product = 380 bp); and for *Dmp1-cre*: W2, 5′-GCCCCTGGACACTGACCATAGC-3′ and W4, 5′-CTGTTCCTCACTCTCACTGTCC-3′ (product = 540 bp). For sexing, two primers were used (20): P1, 5′-CTGAAGCTTTTGGCTTTGAG-3′ and P2, 5′-CCACTGCCAAATTCTTTGG-3′ (male = 331 and 302 bp, female = 331 bp). PCR products were evaluated by electrophoresis on 2.1% agarose gels followed by staining with ethidium bromide and digitally imaged with a Fuji LAS4000 charge-coupled device detector.

Analysis of MBTPS1 Protein from Muscle and Bone—Forelimbs and tibiae from control and *Mbtps1* cKO mice were dissected free of soft tissues, then frozen in liquid nitrogen, and pulverized in a bone mill. Bone powder was then washed extensively with PBS to remove marrow cells and blood prior to extraction at 4 °C by mixing for 72 h with 0.1 M Tris acetate buffer, pH 7.4, containing 8 M urea, 0.2% CHAPS, 0.5 M EDTA, and 0.02% sodium azide. A ratio of 20 ml of extraction solution/g of bone powder was used. After clarification of the extracts by centrifugation, supernatant fractions were dialyzed separately first against distilled water and then against two changes of 5% acetic acid at 4 °C. Extracts were then lyophilized to dryness in several aliquots. Following protein quantitation using the Geno Technology Non-Interfering Protein Analysis Assay kit, samples were hydrated with SDS-PAGE sample buffer and an excess of dithiothreitol and heated at 95 °C for 10 min. 52 μg of bone extracts were electrophoresed per lane of 4–20% linear gradient SDS gels (Precise Tris-HEPES gels, Pierce) at 50 V for 2.5 h and then electroblotted onto PVDF membrane at 100 V for 2 h. Coomassie Blue prestained globular protein standards were also electrophoresed on each gel. Blots were processed for immunodetection with rabbit anti-human or mouse MBTPS1 C-terminal primary antibodies (21) using a SuperSignal West Femto Maximum Sensitivity Chemiluminescent Substrate kit (Thermo Scientific) as described previously (13). Blots were digitally imaged using a Fuji LAS4000 system with a charge-coupled device camera.

Soleus muscles of control and *Mbtps1* cKO mice were used for contractility studies and then immediately flash frozen in liquid nitrogen and stored at −80 °C. Tissues were then homogenized, and the total protein was isolated using radioimmune precipitation assay buffer (Sigma-Aldrich) according to the manufacturer's instructions. The lysates were centrifuged at 12,000 rpm for 10 min at 4 °C, and the supernatants were collected. The protein concentration of the lysates was detected using a Micro BCA Protein Assay kit (Pierce). The lysate and sample buffer were then mixed and boiled for 10 min before loading onto the gel. Proteins (20 and 40 μg/lane) were separated on a Mini-PROTEIN precast gel (Bio-Rad) under constant voltage (200 V) and then transferred electrophoretically to a nitrocellulose membrane by using the Trans-Blot Turbo transfer system using the TGX gel program (Bio-Rad). Membranes were blocked in 5% nonfat dry milk at 4 °C and then incubated with the primary antibody (anti-Mbtps1 C-terminal antibody (21)) overnight at 4 °C. Blots were incubated with secondary antibody (goat anti-rabbit IgG, HRP conjugate (1:20,000); EMD Millipore, Billerica, MA) for 2 h at room temperature and then visualized as noted above for bone extracts.

Immunohistochemical Analysis of Myosin Heavy Chains—Soleus muscles and extensor digitorum longus muscles (EDL) were dissected immediately after sacrifice and flash frozen in optimum cutting temperature medium for storage. Muscles were cut into 14-μm-thick sections using a cryostat and then processed for immunofluorescence staining using a protocol

adapted from that published by Phillips *et al.* (22). Briefly, sections were air-dried, acetone-fixed, and then blocked with mouse M.O.M. IgG blocking reagent (Vector Laboratories, Inc.) for 1 h at room temperature. After washing in PBS, sections were incubated overnight in the following mixture of primary antibodies dissolved in PBS containing 2% normal goat serum: 1:100 anti-type I myosin heavy chain (BS.D5 IgG2b, Developmental Studies Hybridoma Bank), 1:200 anti-type IIA myosin heavy chain (SC.71 IgG1, Developmental Studies Hybridoma Bank), and 1:100 anti-type IIB myosin heavy chain (BF.F3 IgM, Developmental Studies Hybridoma Bank). After washing in PBS, sections were treated for 2 h with the following mixture of secondary antibodies dissolved in PBS containing 2% normal goat serum: Alexa Fluor 647-conjugated goat anti-mouse IgG2b (Invitrogen), Alexa Fluor 488-conjugated goat anti-mouse IgG1 (Invitrogen), and Alexa Fluor 594-conjugated goat anti-mouse IgM (Invitrogen). After washing extensively with PBS, sections were postfixed in methanol for 5 min, rinsed in PBS, and then coverslipped with mounting medium including DAPI (Vector Laboratories, Inc.). Sections were imaged using an inverted Nikon TE2000-E epifluorescence microscope and Metamorph software. ImageJ software was used to overlay different colored images of the same field, and then contrast and brightness were adjusted in Photoshop.

Measurement of Food Intake—Mice were housed individually in Tecniplast metabolic cages for 6 days. The first 3 days represented an acclimatization phase. Daily food intake, urine output, body weight, and solid waste output were then measured for the 2-day period from days 4 to 6, which were considered the study period. All mice were returned to normal caging at the end of the study period.

Isolation of Osteocyte-enriched Bone and Extraction of Proteins for Analysis—Three cKO male mice, two control littermates, and two wild type male mice aged 10 months were processed separately via the procedure described below to obtain osteocyte-enriched bone matrix. Mice were cervically dislocated and sprayed with 70% ethanol prior to dissection of the femora, tibiae, humerus, ulna, and radius while leaving the end of joints intact. Feet were removed from forelimbs and hind limbs distal to the ankle joints and placed in α-minimum Eagle's medium containing penicillin/streptomycin in a laminar flow hood. Limbs were sequentially passed through four dishes of sterile PBS to dilute possible contaminants and then placed in α-minimum Eagle's medium. Each limb was then dissected carefully in a small amount of medium, removing muscle, tendons, and ligaments from the still intact joints. Femora were separated from tibiae, and "clean" bones were placed in α-minimum Eagle's medium. Both ends of each bone were cut off using a scalpel, and the marrow was flushed out using PBS. Dissected bones were then placed in α-minimum Eagle's medium and split longitudinally with a scalpel, and after cutting into 1.5–2.0-mm sections, the pieces were divided into 2 wells of a 6-well culture dish containing PBS. Bone pieces were monitored microscopically throughout the digestion protocol. For Digest 1, the PBS was removed, and the bone pieces were treated with 4 ml of collagenase (2 mg/ml) for 30 min at 37 °C. Cells released were removed, the bone pieces were rinsed with 2 ml of Hanks' balanced salt solution, and the collagenase digestion step was repeated twice more before the bone chips were incubated with 5 mM EDTA and 0.1% BSA in PBS for 30 min at 37 °C. Cells released were removed. The bone chips were then rinsed with 2 ml of Hanks' balanced salt solution and retreated with collagenase for 30 min at 37 °C to obtain an "osteocyte-enriched bone" fraction.

The osteocyte-enriched bone fraction was immediately incubated for 1 h at 4 °C with 0.4 mM AEBSF in PBS to block autolysis of MBTPS1 prior to freezing at −80 °C. Bone chips (0.2–0.3 g) derived from each mouse were then pulverized individually in liquid nitrogen into small particles and resuspended in 10 ml 0.1 M Tris acetate buffer, pH 7.5, containing 8 M urea, 0.5 M EDTA, and 0.2% CHAPS. Each sample was heated initially at 95 °C for 10 min to inactivate degradative enzymes and then extracted for 3 days at 4 °C with mixing. The extracts were then desalted by dialysis in 3500-molecular weight-cutoff tubing against two changes of deionized water and then four changes of 5% acetic acid at 4 °C. Protein content of extracts was determined with the Non-Interfering Protein Analysis Assay kit. Proteins were solubilized in SDS- and 8 M urea-containing sample buffer and electrophoresed under reducing conditions on 4–20% gradient gels (Precise, Thermo Fisher) as described previously (13). Gels were then electroblotted onto PVDF membranes in a CAPS/MeOH buffer, pH 11.0 and subjected to immunodetection with a 1:20,000 dilution of primary antibody recognizing the C-terminal domain of MBTPS1 (21). Chemiluminescence signals were generated using HRP-conjugated goat anti-mouse IgG (Bio-Rad) and SuperSignal West Femto Chemiluminescent Substrate (Pierce). Digital images were collected using a Fuji LAS4000 imager.

Three-point Bending to Failure—To characterize the biomechanical properties of the bones, displacement-controlled three-point bending to failure tests were conducted on excised femora *ex vivo*. Femora were harvested from freshly euthanized mice. For each femur, all associated soft tissue was removed, and the bone was individually wrapped in saline-soaked gauze and then stored at −20 °C until testing. On the day of testing, samples were removed from −20 °C storage and allowed to thaw and reach room temperature. Prior to and throughout the tests, bone samples were kept hydrated with saline-soaked gauze and not allowed to dry out. The femora were placed into the test fixtures so they would be impacted in what would be the anterior to posterior direction *in vivo* (ElectroForce 3200, Bose Corp., Minnetonka, MN). Cross-head displacement and axial load were recorded at a rate of 70 Hz. The stiffness and ultimate force were calculated from the resulting load *versus* displacement curves for each sample. The Young's modulus (E) for each bone was calculated using the following equation.

$$E = \frac{SL^3}{48I} \qquad \text{(Eq. 1)}$$

where S is the stiffness, L is the span length, and I is the area moment of inertia. The area moment of inertia was calculated across the midspan at the fracture location using 10 slices midspan of the realigned microCT scans using the BoneJ plug-in for the image-processing program ImageJ (National Institutes of Health, Bethesda, MD) (23, 24).

MicroCT Analyses on Bone—MicroCT scans were made on isolated femora using a Scanco Vivact 40 instrument. The instrument was calibrated weekly using a series of hydroxyapatite phantoms. Cortical and trabecular bone content was determined using three-dimensional reconstructed bone volume, proprietary software, and standardized protocols with a threshold of 260 g/cm^2. For example, cortical content was assessed using a 50-μm-thick cross-section extending distally from the base of the third trochanter, which was used as an anatomical landmark. Trabecular content was estimated using a 100-μm-thick cross-section of the proximal growth plate containing exclusively secondary spongiosa. Values for total volume, bone volume, hydroxyapatite content per total volume, and hydroxyapatite content per bone volume were obtained from these analyses.

Ex Vivo Muscle Function Studies—Intact EDL and soleus from mice of each genotype were used for collection of isometric force data using an eight-chambered system (25, 26). Experiments were collected and analyzed with ADInstruments PowerLab software customized for these experiments. Muscles were first equilibrated for 20 min to mimic conditions of normal activity (low duty cycle, ~1%). They were then subjected to the length-force relationship test to determine optimal length at which maximal force is achieved. Muscles were stimulated with frequencies ranging from 1 to 130 Hz to generate force *versus* frequency relationships. From the force *versus* frequency, the frequency producing maximal tetanic force (T_{max}) was then used for the rest of the experiments. Muscles were stimulated every minute with T_{max} for 5–10 min to assure that the preparation was stable at which point the tissue bathing buffer was replaced with one containing 0 mM Ca^{2+} + 0.1 mM EGTA. The muscles were then stimulated every minute at T_{max} to determine the impact of removal of external calcium on muscle force. After 20 min, the 0 mM Ca^{2+}buffer was washed out and replaced by a buffer containing 2.5 mM Ca^{2+}, and the muscles were stimulated every minute for 20 min at T_{max} to allow for force recovery. The muscles were then were subjected to fatiguing stimulation protocols that mimic physiological fatigue (50% duty cycle; intermittent fatigue) (27, 28). At the end of fatigue, muscles were allowed to recover by switching the stimulation parameter to a 1-min interval. At the end of a 30-min recovery period, muscles were treated with 5 mM caffeine, which effectively releases calcium from the sarcoplasmic reticulum to test in the intact whole muscle whether excitation-contraction coupling was defective at the end of the recovery process in any of the genotypes.

After force protocols, muscle dimensions and masses were measured for determination of cross-sectional normalized forces and for comparative morphometric analyses. After coating lightly in optimum cooling temperature medium, isolated muscles were flash frozen in liquid N_2-cooled isopentane, sectioned frozen, and then analyzed for general histology by hematoxylin staining or for myosin heavy chain expression by immunofluorescence staining.

Isolation of Muscle and Osteocyte-enriched RNA, Labeling, and Processing for Whole Genome Array—Osteocyte-enriched mouse bone chips were prepared as described above and then treated sequentially four times with alternating EDTA treatments followed by collagenase digestions. Total RNA was isolated from frozen bone chips and from flash frozen muscle samples using an RNeasy Micro kit according to standard protocols along with the inclusion of a proteinase K digestion step. The RNA was analyzed for quality using a Nanodrop and an Agilent Bioanalyzer after which 100 ng of total RNA were used for the Agilent Mouse Transcriptome Array 1.0 protocol. Briefly, the total RNA was primed with primers containing a T7 promoter sequence. Single-stranded cDNA was synthesized with a T7 promoter sequence at the 5′-end, converted to double-stranded cDNA, and *in vitro* transcribed with T7 RNA polymerase to generate antisense RNA. The cRNA was cleaned up using a bead protocol and then used to synthesize sense strand cDNA in a reaction that included dUTP at a fixed ratio relative to dTTP. RNase H was used to hydrolyze the cRNA strand after which the sense strand cDNA was purified using beads and then fragmented at the unnatural dUTP residues using uracil-DNA glycosylase and apurinic/apyrimidinic endonuclease 1. The fragmented cDNA was labeled by terminal deoxynucleotidyltransferase using the Affymetrix proprietary DNA Labeling Reagent that is covalently linked to biotin. The biotinylated and fragmented cDNA was hybridized overnight to the Mouse Transcriptome 1.0 arrays after which it was washed and stained on a FS450 GeneChip system and scanned using a GCS30007G scanner.

The CEL files from muscle or bone osteocytes then were analyzed using Affymetrix Expression Console and Transcriptome Analysis Console 2.0. For detailed statistical analysis, the CEL files were imported into GeneSpring v13, quantile-normalized using the PLIER16 algorithm, and baseline-transformed to the median of all samples. The $\log_2$-normalized signal values were then filtered to remove entities that showed signal in the bottom 20th percentile across all samples. The above lists were subjected to a *t* test ($p < 0.05$) with a Benjamini-Hochberg false discovery rate correction. A 1.5-fold filter was applied to identify genes that were differentially expressed between control and cKO mice.

Quantitative PCR—Flash frozen muscle was disrupted in TRIzol reagent using a miniature motorized homogenizer. Total RNA was then isolated using a Direct-zol RNA MiniPrep Plus column (Zymo Research) and amplified using a High Capacity RNA to cDNA kit (Applied Biosystems). *Mbtps1* and *cre* recombinase were quantitated using TaqMan Universal Master Mix II with uracil *N*-glycosylase (Applied Biosystems) and 6-carboxyfluorescein-labeled/minor grove binding probes and normalized relative to β-actin or *Gadph*.

Results

Mbtps1 mRNA and Protein Are Deleted in Osteocyte-enriched Bone but Not Skeletal Muscle—cKO bone osteocytes exhibited a ~70% reduction in *Mbtps1* mRNA (array data deposited at NCBI under accession number GSE69975). In terms of protein, osteocyte-enriched control bone extracts contained an 18-kDa MBTPS1 fragment band also enriched in laser microscope-dissected biomineralization foci (Fig. 1*a*), sites of initial deposition of hydroxyapatite in osteoblastic cultures (29).

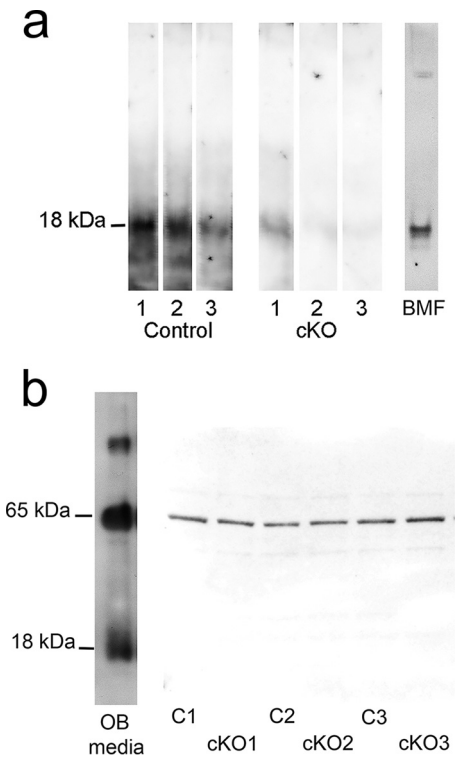

FIGURE 1. **Western blotting for MBTPS1 in bone and soleus muscle extracts.** SDS-polyacrylamide gel electrophoresis and Western blotting are described under "Experimental Procedures." *a*, extracts of AEBSF-treated osteocyte-enriched bone from *Dmp1-cre Mtps1* cKO mice contain reduced amounts of the 18-kDa-molecular mass fragment compared with controls. *Control*, bones from three separate control littermate mice; *cKO*, bones from three knock-out mice; *BMF*, biomineralization foci isolated by laser capture microdissection from AEBSF-treated osteoblastic cultures (29). *b*, muscle extracts from cKO and control SOL were indistinguishable when immunoblotted for MBTPS1. *C1–C3*, soleus muscles from three littermate controls; *cKO1–cKO3*, soleus muscles from three knock-out mice; *OB media*, osteoblast-derived culture media. Both immunoblots were treated with a monospecific polyclonal antibody reacting with the C-terminal region of mouse MBTPS1 (a gift from Dr. N. G. Seidah). Similar blotting results were obtained with a second anti-human MBTPS1 antibody (not shown). Lanes for biomineralization foci and culture media are provided for comparative purposes and were not imaged at the same time as bone or muscle extracts.

Other work[4] has shown that the relative content and half-life of this 18-kDa fragment in bone cells is increased after treatment with AEBSF, which blocks autolytic cleavage of MBTPS1. Consistent with cre recombinase-mediated deletion of *Mbtps1*, the 18-kDa MBTPS1 band is barely detectable in two of three *Mbtps1* cKO bone extracts and noticeably reduced in a third specimen (Fig. 1*a*).

To determine whether *Dmp1-cre* was "leaky" in skeletal muscle, adult cKO and control soleus muscles (SOL) and EDL were processed for quantitative PCR. However, the relative content of *Mbtps1* mRNA was not statistically different from that in littermate controls (Table 1). Whole genome arrays on SOL from four *Mbtps1* cKO and control mice independently confirmed these findings (deposited at NCBI under accession number GSE69985). Furthermore, the expression of *cre* recombinase was also determined in adult cKO SOL and cKO EDL. Interestingly, no ($n = 4$) or low ($n = 3$) levels of *cre* were detected in cKO mice (Table 2). In contrast, β-actin and *Gadph* (not shown) expression was robust in all muscles tested. Where expressed, *cre* was present in both EDL and SOL from the same animal despite the fact that the muscle phenotype (see below) was restricted to cKO SOL. *cre*/actin Ct ratios for cKO EDL and cKO SOL were statistically indistinguishable (Table 2).

We next asked whether the content of MBTPS1 protein was reduced in cKO SOL. Similar to the mRNA data, the content of an additional immunoreactive 65-kDa-molecular mass MBTPS1 fragment was unchanged when extracts from three separate cKO and littermate control soleus muscles were compared (Fig. 1*b*). A similar 65-kDa fragment is consistently observed in the medium fraction of osteoblastic cell cultures (Fig. 1*b*). Therefore, it is apparent that the 18-kDa fragment is enriched in bone osteocytes, whereas the 65-kDa form is present in muscle. Although MBTPS1 is a membrane-bound protease localized to the cis/medial Golgi, a soluble form can also be shed into the medium of kidney cells (30) and bone cells (13).

Long Bones from Adult Mbtps1 cKO Mice Are Stiffer but Not Different in Bone Mineral Content—In view of our use of bone-restricted *Dmp1-cre*, we initially carried out microCT scans on skeletons of *Mbtps1* cKO and control mice. Surprisingly, when microCT data from adult tibiae were compared, no significant differences were found in mineral density, cortical thickness, trabecular number, trabecular density, trabecular thickness, bone volume/total volume, trabecular spacing, bone mineral density, or mineral content (Tables 3 and 4). To analyze biomechanical properties, three-point bending studies were also carried out on isolated femora. Importantly, Young's modulus for cKO femora averaged 7.38 ± 1.65 (mean ± S.D.) compared with 5.90 ± 0.92 for controls, a 25% increase in stiffness ($p = 0.013$). Because mineral densities were similar (Table 4), we hypothesize that this increase in stiffness reflects a change in organic bone matrix composition. Although neonatal *Dmp1-cre Mbtps1* cKO mice did not display a bone phenotype (not shown), we did note a characteristic increase in body weight starting abruptly at 15–20 weeks of age, the time at which the mouse approaches skeletal maturity (Fig. 2, *a–d*). However, when weight data from all litters were pooled at 10–12 months, *Mbtps1* cKO males weighed on average only 1.5 ± 5.9 g more than controls ($p = 0.320$). Because initial analyses of whole body fat could not account for this difference between *Mbtps1* cKO and control mice (data not shown), we analyzed skeletal muscle and found the source of this weight gain.

Adult Mbtps1 cKO SOLs Are Larger and Contract More Forcefully Even When Normalized for Size—SOL and EDL, prototypical slow twitch and fast twitch muscles, respectively, were isolated from adult mice and subjected to contractile studies *ex vivo* (Fig. 3*a*). cKO SOLs were 12% larger in mass ($p = 0.02$) (Fig. 3*b*) and quantitatively longer in length (data not shown). Interestingly, cKO SOL were also 30% stronger than control littermates both in terms of relative and specific contractile force ($p < 0.05$) (Fig. 3, *c*, *d*, and *e*). In contrast, when comparable studies were carried out on adult EDL from cKO and control littermates, no significant differences were observed in size, length, and contractile force (Fig. 3, *b*, *f*, and *g*, and data not shown).

The force-frequency curve for *Mbtps1* cKO SOL was also shifted to the right of the control by a small but significant amount; *e.g.* at the lower frequencies, a higher frequency stim-

[4] J. P. Gorski and N. T. Huffman, unpublished data.

TABLE 1

Quantitative PCR for *Mbtps1* in cKO and control soleus and EDL muscle using relative standard curve method

Data represent means ± S.D.

10-month-old mice	*Mbtps1* cKO/actin	*Mbtps1* control/actin	Student's *t* test
Soleus muscles (n = 3)	1.13 ± 0.47	1.23 ± 0.32	p = 0.30
EDL muscles (n = 3)	1.16 ± 0.43	1.27 ± 0.38	p = 0.37

TABLE 2

Quantitation of *cre* recombinase expression in cKO EDL and cKO SOL muscles by quantitative PCR

ND, not determined.

cre-positive *Mbtps1* cKO mice					*cre*-negative *Mbtps1* cKO mice			
	Ct					Ct		
Mouse ID	EDL	SOL	Actin	*cre*/actin	Mouse ID	EDL	SOL	Actin
616	33.52 ± 0.23		27.00 ± 0.031	1.24 ± 0.23	602	ND		27.21 ± 0.064
616		34.68 ± 0.28	26.76 ± 0.081	1.25 ± 0.32	602		ND	25.93 ± 0.034
617	34.01 ± 0.19		26.49 ± 0.14	1.28 ± 0.23	762	ND		27.82 ± 0.25
617		34.56 ± 0.52	26.72 ± 0.05	1.34 ± 0.54	762		ND	26.42 ± 0.018
764	35.62 ± 0.25		27.48 ± 0.16	1.30 ± 0.30	781	ND		27.00 ± 0.42
764		34.28 ± 0.15	25.76 ± 0.09	1.33 ± 0.17	678		ND	27.48 ± 0.31

TABLE 3

Bone parameters from 10–11-month-old *Dmp1-cre Mbtps1* cKO and control mice are indistinguishable

Data represent means ± S.D. BV/TV, bone volume/total volume.

	Mineral density	Cortical thickness	Trabecular number	Trabecular density	Trabecular thickness	BV/TV	Trabecular spacing
cKO (n = 9)	1190.403 ± 25.149	0.245 ± 0.0151	1.267 ± 0.596	868.302 ± 28.887	0.0506 ± 0.0097	0.0888 ± 0.0679	1.065 ± 0.925
Control (n = 9)	1188.947 ± 14.061	0.246 ± 0.0167	1.390 ± 0.783	880.442± 48.153	0.0558 ± 0.0118	0.0814 ± 0.0581	0.974 ± 0.785
p value	0.881	0.884	0.712	0.526	0.318	0.807	0.824

TABLE 4

Long bones from adult *Mbtps1* cKO mice are stiffer but are not different in mineral content or length

Data represent means ± S.D. BMD, bone mineral density.

10–12-month old mice	Femur BMD	Mineral content	Femur length	Femur diameter	Young's modulus
	g/cm^2	*% ash weight*	*mm*	*mm*	
Dmp1-cre Mbtps1 cKO (males)	0.0616 ± 0.003 (n = 6)	63.38 ± 4.17 (n = 15)	16.73 ± 0.320 (n = 15)	3.04 ± 0.142 (n = 7)	7.384 ± 1.65, 25% increase (n = 9)
Control littermates (males)	0.0646 ± 0.003 (n = 5)	63.22 ± 4.85 (n = 17)	16.57 ± 0.48 (n = 21)	3.02 ± 0.243 (n = 7)	5.898 ± 0.918 (n = 13)
Statistics, two tailed *t* test	p = 0.167	p = 0.880	p = 0.142	p = 0.841	p = 0.0134

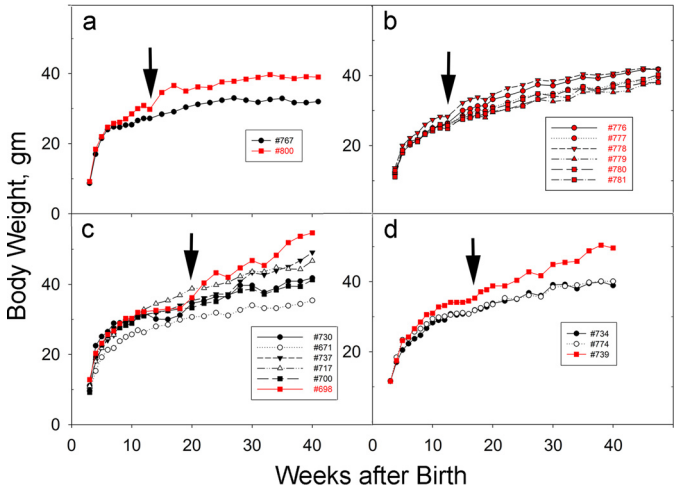

FIGURE 2. ***Mbtps1* cKO male mice exhibit weight gain upon reaching skeletal maturity (15–20 weeks).** Growth curves for individual male mice from four representative litters (*a*, *b*, *c*, and *d*) are depicted from 3 weeks to at least 40 weeks of age. *Black arrows* indicate the time at which the increased growth rate of cKO mice was detected within individual litters. *Red symbols*, cKO mice; *black* and *white symbols*, control littermates. *gm*, grams.

ulation is required to elicit the same maximal tetanic force as control SOL (Fig. 4*a*). In contrast, the responses of control and *Mbtps1* cKO SOL were similar when fatigued and then challenged with caffeine (Fig. 4*b*) and upon depletion and replenishment of extracellular calcium (Fig. 4*c*). Force-frequency curves for control and *Mbtps1* cKO EDL were indistinguishable (Fig. 4*d*) as were the results of fatigue and extracellular calcium depletion protocols (Fig. 4, *e* and *f*). In view of these changes in adult *Mbtps1* cKO SOL, we asked whether young *Mbtps1* cKO SOLs were also larger and more powerful than littermate controls.

Young Mbtps1 cKO SOLs Are Not More Powerful than Controls—Because *Dmp1-cre Mbtps1* cKO mice exhibited an increase in weight gain at 15–20 weeks (Fig. 2), we asked whether this finding reflected the temporal onset of the muscle phenotype. Contraction studies were carried out on isolated SOL and EDL from young *Mbtps1* cKO and control mice (Fig. 5) at 12 weeks of age, just prior to this observed increase in body weight. Based on this functional testing, cKO and control SOLs were not different in terms of size, force frequency relationship, contractile force, or fatigue properties (Fig. 5, *a*–*e*). Large error bars associated with contractile measurements in young SOL are likely due to a developmentally immature excitation-contraction coupling apparatus (31). However, young cKO EDL was about 25% more powerful than control EDL (Fig. 5*h*), a difference that did not persist in adults (Fig. 3, *f* and *g*).

Adult cKO SOLs Exhibit Centralized Nuclei, a Morphological Characteristic of Regenerating Muscle—Fig. 6 shows representative views of hematoxylin- and eosin-stained adult SOL from control and *Mbtps1* cKO animals. *Black arrows* mark the posi-

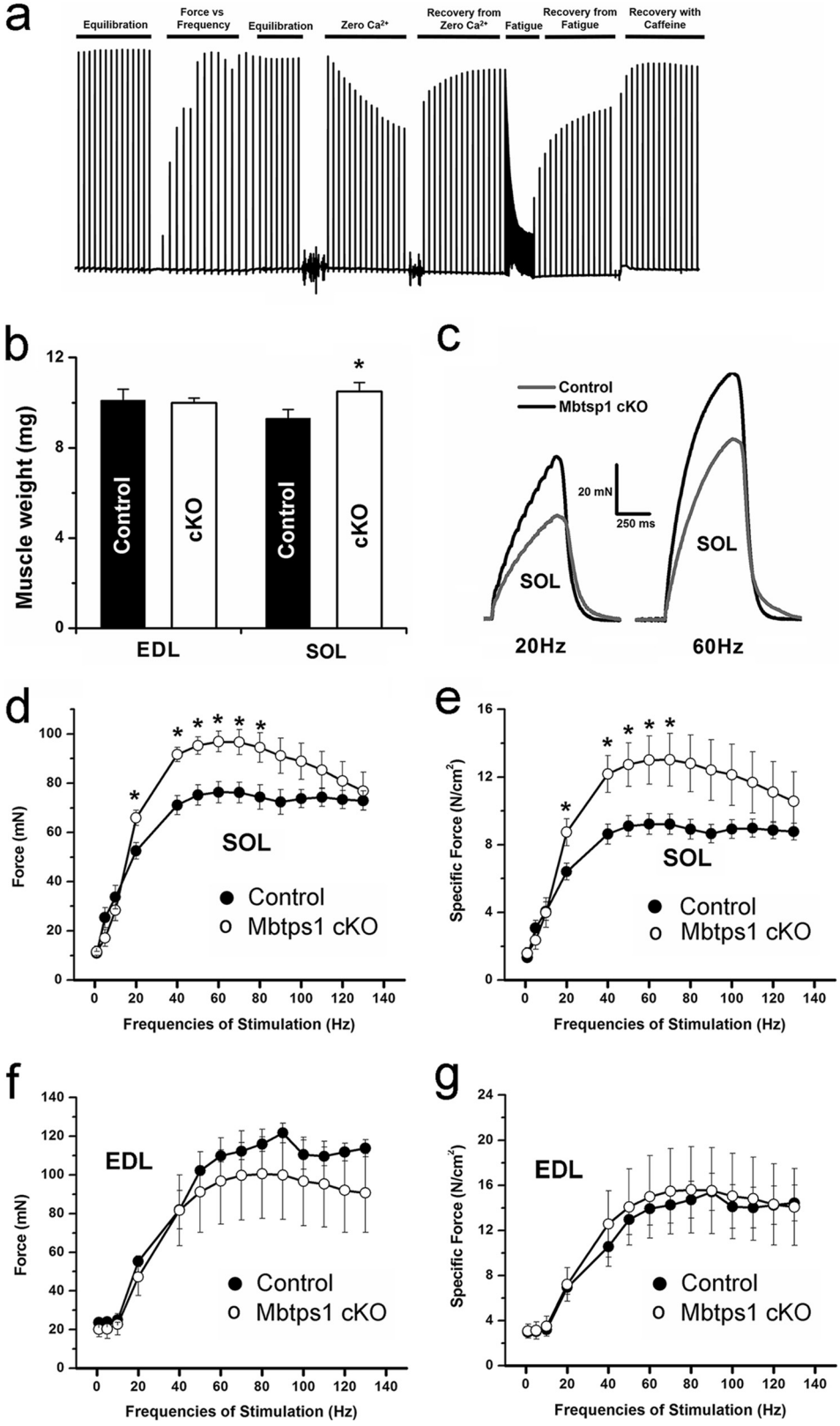

FIGURE 3. **Soleus muscles but not EDL muscles from adult *Mbtps1* cKO mice are bigger and produce more contractile force.** *a*, representative data tracing of the *ex vivo* contractility assay obtained from individual muscles. Intact EDL and soleus muscles were mounted between two platinum electrodes and stimulated with non-tetanic and tetanic voltage trains to induce muscle contraction (*y axis*, contractile force; *x axis*, time.) *b*, EDL and soleus muscle wet weights from control and *Mbtps1* cKO mice. *c*, force tracings of submaximal (*left*) and maximal (*right*) tetanic contractions of intact soleus muscles from control (*gray line*) and *Mbtps1* cKO (*black line*) mice stimulated *ex vivo*. *d*, soleus muscle contractile force (millinewtons (*mN*)) from control mice and *Mbtps1* cKO mice at increasing frequencies of stimulation in the range of 1–130 Hz. *e*, soleus muscle contractile forces from *d* normalized to cross-sectional area of the muscle (newtons (*N*)/cm^2). *f*, contractile force (millinewtons) of intact EDL muscles from control and *Mbtps1* cKO mice stimulated at frequencies of 1–130 Hz. *g*, EDL muscle forces from *f* normalized to muscle cross-sectional area (newtons/cm^2). Data are represented as mean ± S.E. (*error bars*). * denotes significant difference ($p < 0.05$) when compared with control.

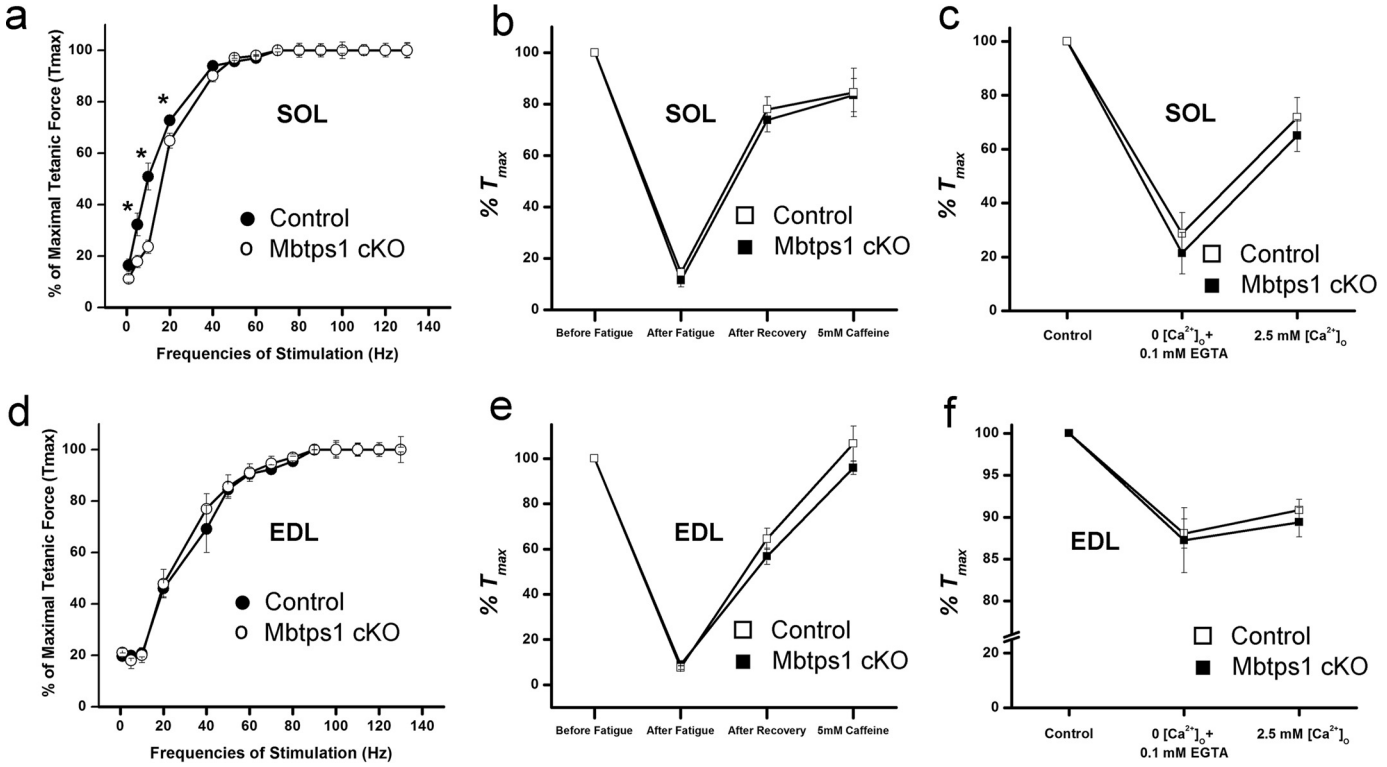

FIGURE 4. **Soleus muscles from adult *Mbtps1* cKO mice display rightward shift of force-frequency relationship.** *a*, force *versus* frequency curves of soleus muscles from control and *Mbtps1* cKO mice stimulated with frequencies ranging from 1 to 130 Hz. Force is normalized to maximum muscle force (T_{max}) and expressed as a percentage. *b*, relative contractile force of soleus muscles from control and *Mbtps1* mice after a fatigue-inducing stimulation protocol and after a recovery period of non-fatiguing tetanic stimulations in both the absence and presence of 5 mM caffeine. Data are expressed as a percentage of force produced by the muscle prior to fatigue. *c*, relative contractile force of soleus muscles from control and *Mbtps1* cKO mice contracted under external conditions of 0 $[Ca^{2+}]_o$ and after replenishment of 2.5 mM $[Ca^{2+}]_o$ for force recovery. Data are expressed as a percentage of force produced by the muscle prior to removal of $[Ca^{2+}]_o$. *d*, EDL muscle force *versus* frequency (1–130 Hz) curves from control and *Mbtps1* cKO mice. Contraction force is normalized to T_{max} of the muscle and expressed as a percentage. *e*, EDL muscle relative contractile force from control and *Mbtps1* mice after a fatigue-inducing stimulation protocol and after a recovery period of non-fatiguing tetanic stimulations in both the absence and presence of 5 mM caffeine. Data are expressed as a percentage of force produced by the muscle prior to fatigue. *f*, EDL muscle relative contractile force from control and *Mbtps1* mice contracted in external conditions of 0 $[Ca^{2+}]_o$ and after washout with 2.5 mM $[Ca^{2+}]_o$ for force recovery. Data are expressed as a percentage of force produced by the muscle prior to removal of $[Ca^{2+}]_o$. Data are represented as mean ± S.E. (*error bars*). * denotes significant difference ($p < 0.05$) when compared with control.

tions of centralized nuclei (Fig. 6). It is apparent that bigger and more forceful cKO SOLs are enriched in myofibers with central nuclei (21.5 ± 5.7%, mean ± S.D.), whereas control SOL muscles contain background levels (3.5 ± 2.9%, $p > 0.001$). A long standing correlation of centralized nuclei with muscle regeneration (32–36) was recently challenged by inconsistent findings in some transgenic muscle models (37, 38). However, our results strongly support an association with muscle regeneration because *Mbtps1* cKO EDLs, which are phenotypically unaffected, contain only background levels of central nuclei (4.0 ± 2.9%) (Fig. 6, *c* and *d*).

Young Mbtps1 cKO SOLs Are Not Enriched in Centralized Nuclei—Myofibers from young *Dmp1-cre Mbtps1* cKO SOL and control muscles contain few centralized nuclei (Fig. 6, *e–h*). Quantitatively, only 3.4% ± 3.2 of myofibers in cKO SOL contained centralized nuclei, which was not different from that for control SOL (3.4 ± 2.2%, $p = 0.989$). Likewise, the content of centralized nuclei in young *Mbtps1* cKO and control EDL were indistinguishable and similar to background levels (5.2 ± 2.1 *versus* 5.2 ± 3.5%).

Myofibers Exhibiting Centralized Nuclei Preferentially Express Type I Myosin Heavy Chain—To evaluate their distribution within SOL and EDL, type I, type IIA, and type IIB myosin heavy chains were immunofluorescently stained in frozen sections of adult *Mbtps1* cKO and control muscles. Consistent with a published report (39), the composition of slow twitch control SOL was composed of 41.8% type I+-expressing myofibers (*magenta* in color) and 54.5% type IIA+-expressing myofibers (*green* in color) (Fig. 7*a* and Table 5). A small percentage of myofibers also stained for type IIB (3.8%), but these were absent from cKO SOL (Fig. 7*b*). DAPI-stained nuclei appear *yellow* in this image and were flattened around the inside periphery of most control myofibers (Fig. 7*a*). Importantly, 15.8% of type I myosin heavy chain-positive cells express central nuclei in cKO SOL muscles (Fig. 6*b*, *arrows*, *magenta*-colored myofibers), whereas, by comparison, only 3% of type IIA-expressing cells contain central nuclei (Table 5). The sum of these two numbers (18%) agrees well with our prior estimate of 21.5% for cKO SOL after H&E staining (see Fig. 6*b*). cKO SOL contained similar amounts of type I+ myofibers and fewer type IIA+ myofibers (Table 5), despite the fact that a prior report showed that regeneration of injured soleus muscle led to a selective enrichment in type I+ myosin heavy chain myofibers at the expense of type IIA+ and type X+ myofibers (40). Although deficient in type I+ myosin heavy chain myofibers, adult fast twitch EDL cKO and control muscles were indis-

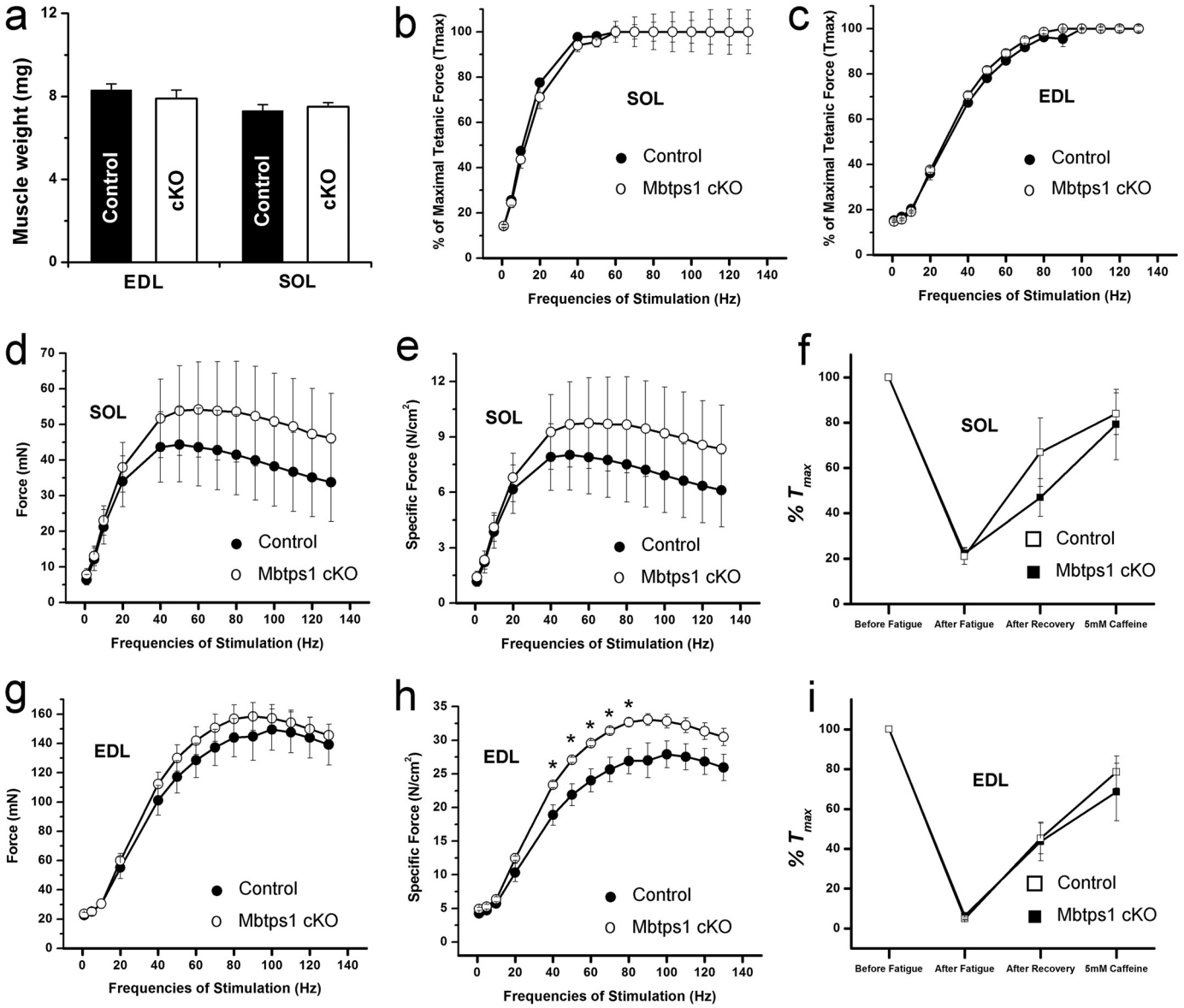

FIGURE 5. **EDL and SOL contractile properties from young control and *Mbtps1* cKO mice.** *a*, EDL and soleus muscle wet weights from control and *Mbtps1* cKO mice. *b*, force *versus* frequency curves of intact soleus muscles from control and *Mbtps1* cKO mice stimulated at individual frequencies ranging from 1 to 130 Hz. Force is normalized to maximum muscle force (T_{max}) and expressed as a percentage. *c*, EDL muscle force *versus* frequency (1–130 Hz) curves from control and *Mbtps1* cKO mice. Contraction force is normalized to T_{max} of the muscle and expressed as a percentage. *d*, soleus muscle contractile force (millinewtons (*mN*)) from control mice and *Mbtps1 cKO* mice at increasing frequencies of stimulation in the range of 1–130 Hz. *e*, soleus muscle contractile forces from *d* normalized to cross-sectional area of the muscle (newtons (*N*)/cm^2). *f*, relative contractile force of soleus muscles from control and *Mbtps1* cKO mice after a fatigue-inducing stimulation protocol and after a recovery period of non-fatiguing tetanic stimulations in both the absence and presence of 5 mM caffeine. Data are expressed as a percentage of force produced by the muscle prior to fatigue. *g*, contractile force (millinewtons) of intact EDL muscles from control and *Mbtps1* cKO mice stimulated at frequencies of 1–130 Hz. *h*, EDL muscle forces from *g* normalized to muscle cross-sectional area (newtons/cm^2). *i*, EDL muscle relative contractile force from control and *Mbtps1* cKO mice after a fatigue-inducing stimulation protocol and after a recovery period of non-fatiguing tetanic stimulations in both the absence and presence of 5 mM caffeine. Data are expressed as a percentage of force produced by the muscle prior to fatigue. Data are represented as mean ± S.E. (*error bars*). * denotes significant difference ($p < 0.05$) when compared with control.

tinguishable in terms of their contents of type IIA, type IIB, and type X myosin heavy chain expressing myofibers (Table 5).

Gene Expression in Bone and Mechanistic Insights Based on Bigger, More Forceful cKO SOL—To begin to determine the molecular mechanisms responsible for the observed bone-muscle cross-talk, whole genome arrays were performed on both muscle and osteocyte-enriched bone. In addition to a ~70% reduction in *Mbtps1* mRNA, knock-out bone osteocytes exhibited a significantly reduced expression of 270 genes with only 10 genes increased relative to littermate controls (data deposited with NCBI under accession number GSE69975). Specifically, osteocyte markers *Mepe*, *Sost*, *Phex*, and *Dmp1* were all reduced 3.0–1.5-fold along with osteoblast-specific periostin and myogenic repressors *Tgf-β1*, *Tgf-β2*, and *Tgf-β3*. Gene profiling identified alterations in several pathways in knock-out bone including TGF-β receptor signaling, TGF-β signaling, adipogenesis, pluripotency, and endochondral ossification (data not shown). Any individual factor or a combination of these factors may be responsible for the enhanced cKO soleus muscle.

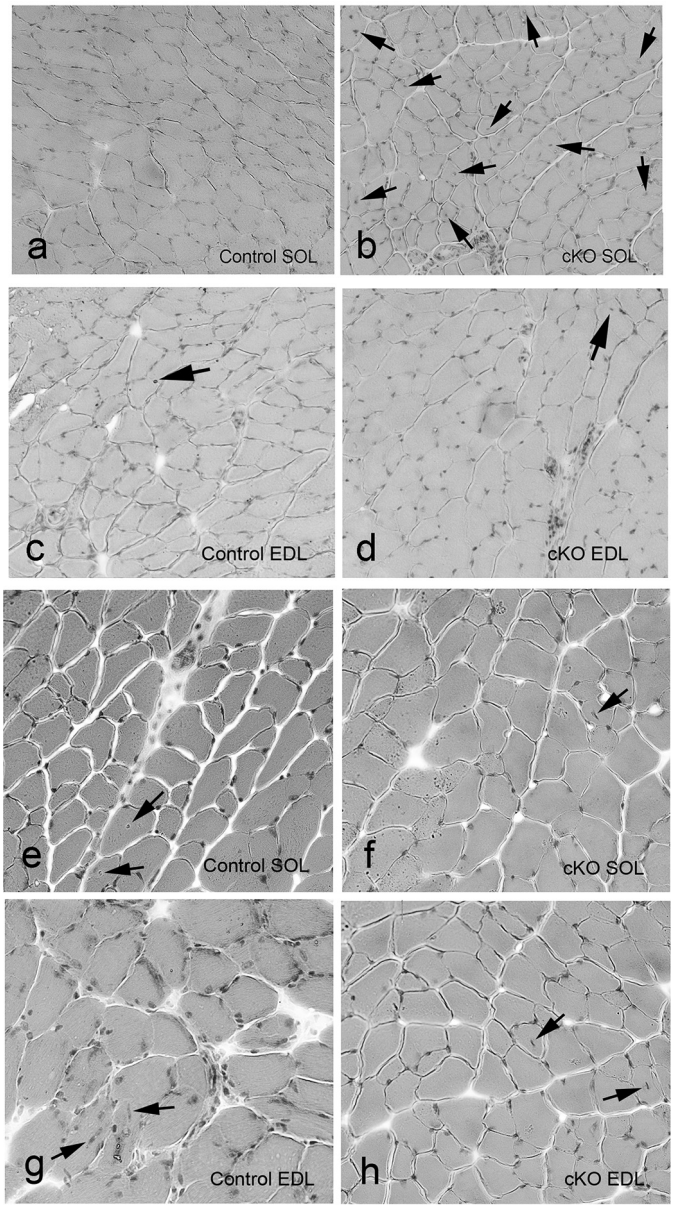

FIGURE 6. **Adult, but not young, *Dmp1-cre Mbtps1* cKO SOLs are enriched in centralized nuclei.** Muscles were dissected immediately following euthanasia and flash frozen in liquid nitrogen, and frozen sections were processed for staining as described under "Experimental Procedures." Representative cross-sectional views of hematoxylin- and eosin-stained SOL and EDL from adults and young mice are depicted in *a–d* and *e–h*, respectively. *a*, adult control SOL; *b*, adult cKO SOL; *c*, adult control EDL; *d*, adult cKO EDL; *e*, young control SOL; *f*, young cKO SOL; *g*, young control EDL; *h*, young cKO EDL. Typical centralized nuclei within these microscopic fields are marked with *black arrows*. Images depicted were photographed at 10× *magnification* and are printed in grayscale.

To identify metabolic changes that may explain the *Dmp1-cre Mbtps1* cKO muscle phenotype, we carried out whole genome arrays on adult SOL (deposited in NCBI under accession number GSE69985). Gene profiling revealed increased expression in pathways mediating EGF receptor signaling, circadian exercise, striated muscle contraction, glycolysis, fatty acid oxidation, and adipogenesis. Briefly, actinin-α3 was elevated in cKO SOL; *Actn3* is a biomarker for increased muscle performance in elite athletes (41). Other striated muscle contraction genes increased included mitsugumin 29 (*Mg29*), vimentin, desmin, and slow twitch muscle-restricted troponin. Embryonic and perinatal myosin heavy chains (*Myh3* and *Myh8*), which have been used as biomarkers to identify muscle regeneration (42–44), were also increased. *Myf6*, which is associated with satellite cell activation during muscle regeneration (45), and *Pax7*, *Myod1*, and myogenin (*Myog*), which are required for postnatal growth and regeneration of adult skeletal muscle (46–48), were also elevated in *Mbtps1* cKO SOL. Metabolically, enhanced expression of triglyceride lipase in cKO SOL should facilitate release and oxidation of fatty acids. Finally, core E-box-dependent circadian clock genes *Per1/2* and *Cry1/2* were elevated in cKO SOL compared with controls, whereas core clock genes *Bmal* (*Arntl*), *Dec1*, and *Dec2* were reduced in cKO SOL muscles, consistent with the known 12-h cycle offset for *Bmal* expression compared with that for *Per1/2* and *Cry1/2* (49). Taken together, the gene expression profile for cKO SOL is consistent with observed changes in size and function and remarkably resembles that for regenerating skeletal muscle.

Discussion

Male *Dmp1-cre Mbtps1* cKO mice display an age-related slow twitch muscle phenotype with increased specific contractile force and size, which implies novel bone-muscle cross-talk signaling. Although microCT analyses revealed no differences in trabecular or cortical bone mineral density or morphological parameters between cKO and control tibiae, three-point bending studies on femora demonstrated a significant 25% gain in stiffness in *Mbtps1*-deficient bone ($p = 0.01$). We rationalize this outcome in terms of a requirement for MBTPS1 for transcription of bone matrix genes including fibronectin, fibrillin2, and collagen XI (13). Because expression was not down-regulated in osteocyte-enriched bone (array data deposited at NCBI under accession number GSE69975), MBTPS1 regulation of these mineralization-related genes may be restricted to osteoblast-like cells (13).

Analysis of muscles from adult *Dmp1-cre Mbtps1* cKO mice revealed several unexpected findings. cKO SOL displayed a 30% greater contractile force, 12% bigger mass, and 6-fold increase in centralized nuclei. Central nuclei are a well known morphological characteristic of regenerating muscle (32–36); however, the effect of conditional deletion of *Mbtps1* in bone was restricted to type I myosin heavy chain-expressing myofibers. We interpret this finding as supporting a regenerative response in cKO SOL but not EDL from the same mice. Furthermore, EDL muscles from the same hosts do not show immunochemical evidence of a fast twitch (type II myosin) to slow twitch (type I myosin) transition (Table 5). The latter finding distinguishes the response of *Dmp1-cre Mbtps1* cKO muscle from that expected after endurance training (50).

Consistent with the morphological data, cKO SOL also expressed elevated levels of *Myod1*, *Myf6*, *Myog*, and *Pax7* along with embryonic and perinatal myosin heavy chain *Myh3* and *Myh8* genes, which postnatally represent independent biomarkers of muscle regeneration (45–49, 51–53). Regeneration of type I+ and type II+ myosin heavy chain-expressing myofibers is regulated differently (54) but originates by activation of distinct populations of satellite cells within each muscle (9, 10).

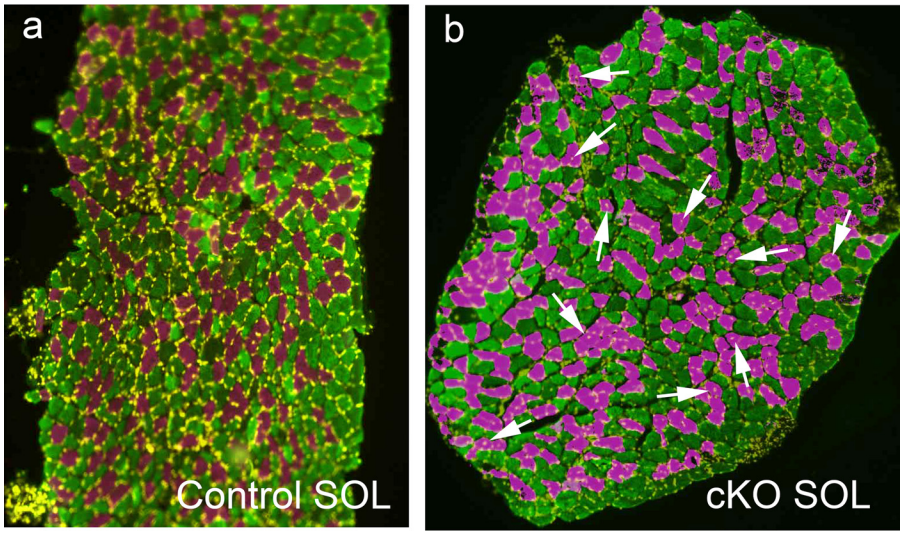

FIGURE 7. **Only type I myosin heavy chain-expressing cKO soleus muscle myofibers exhibit centralized nuclei.** Muscles from adult *Dmp1-cre Mbtps1* cKO and control mice were dissected immediately following euthanasia and flash frozen, and frozen sections were immunostained as described under "Experimental Procedures." Images of whole muscle cross-sections were pseudocolored using ImageJ. cKO soleus muscle is enriched in type I myosin heavy chain-expressing cells (*magenta*-colored myofibers) with centralized nuclei (*white arrows*), whereas type I myosin heavy chain-positive and type IIA heavy chain-positive (*green*-colored myofibers) control cells contain only background levels of centralized nuclei. Nuclei were identified by DAPI staining (*yellow* color). *a*, control soleus muscle; *b*, *Dmp1-cre Mbtps1* cKO muscle. Images shown were photographed at 10× *magnification*. (Please note that average quantitative results of fiber typing and centralized nucleus counts for SOL and EDL muscles for cKO and control muscles are presented in Table 5.)

In contrast to adult mice, the contractile force and size of young SOL cKO and control muscles were indistinguishable, indicating that the response of SOL to deletion of *Mbtps1* in bone occurs after 12 weeks of age.

Although the muscle phenotype is restricted to cKO SOL, analyses of *Mbtps1* mRNA and protein content in cKO SOL were indistinguishable from controls. Also, *cre* recombinase was only detectable in less than half of *Mbtps1* cKO mice. Furthermore, when detected, *cre* expression was equivalent in both cKO EDL and cKO SOL even though changes in muscle function and gene expression were localized to the latter. Taken together, these findings are not consistent with leakiness of the *Dmp1-cre* in cKO SOL but rather support an indirect bone-muscle cross-talk mechanism.

Transgenic models with a muscle phenotype can be classified into two groups: 1) specific contractile force is either unchanged or 2) specific contractile function is decreased. For example, myostatin-null mice gain mass in both their EDL and SOL; however, functional testing shows that specific contractile force is less than controls for myostatin cKO EDL and the same as controls for cKO SOL (55–57). Conditional deletion of IGF-1 in muscle was found to be selective for fast twitch EDL where mass and maximum power increased about 30% (58). However, specific contractile force was the same in transgenic and control EDL muscles. Furthermore, a double knock-out of *Myod* and dystrophin and a knock-out of calpain 3 (59, 60) both display a reduction in muscle contractile force. In contrast, the adult *Dmp1-cre Mbtps1* cKO muscle phenotype represents a special case because SOLs exhibit an increase in both specific contractile force and size.

To identify candidate signaling pathways mediating bone-muscle cross-talk, we compared gene array data for adult bigger and more powerful cKO SOL with that for control SOL. Interestingly, expression of basic helix-loop-helix domain-containing transcriptional regulators *Dec1* (*Bhlhe40*, *Stra13*, *Bhlhb2*) and *Dec2* (*Bhlhe41*, *Sharp1*, *Bhlhb3*) was decreased significantly in cKO SOL compared with controls at the time the mice were euthanized. *Bhlhe40* and *Bhlhe41* are core circadian clock genes that like *Per* and *Cry* are positively regulated by *Bmal* and *Clock* (61, 62); in return, expression of *Dec1* and *Dec2* is subject to negative feedback (62, 63) (Fig. 8*a*). *Dec1* and *Dec2* expression in muscle displays a rhythmic 24–28-h cycle (64), which because of negative feedback regulation would be predicted to be offset by ~12–24 h compared with that for *Bmal* and *Clock* (Fig. 8, *a* and *b*). *Bmal* expression is required for satellite cell activation in muscle regeneration (65). *Dec1*/*Dec2*, in contrast, were shown previously to repress myogenesis *in vitro* and *in vivo* by blocking transcription of *Myod1* as well by altering expression of a number of muscle contractile and mitochondrial proteins (66–68). By analogy with the age-related onset of the *Dmp1-cre Mbtps1* cKO phenotype here, *Dec2*-null mice show no deficit with respect to repair of embryonic muscle; however, as expected for a repressor of myogenesis, regeneration after injury in post-natal *Dec2*(−/−) mice is increased (68). Postnatally, *Dec1* represses *Notch* signaling, which in null mice leads to a complex muscle phenotype (69) (Fig. 8*b*).

Because SOLs in *Dmp1-cre Mbtps1* cKO mice display characteristics of regenerating muscle, we hypothesized that a cycling circadian expression pattern for myogenic repressors *Dec1*/*Dec2* could stimulate or reduce expression of pro- or anti-myogenic genes, respectively, during their "down cycle" (Fig. 8, *a* and *b*). Because Lecomte *et al.* (66) have already identified positive and negative transcriptional muscle-specific targets of *Dec1*/*Dec2*, we asked whether expression of these target genes is temporally correlated with that of transcriptional regulators *Dec1*/*Dec2*? Importantly, the majority of muscle-specific target genes (79 of 110) displayed the predicted response (66) when *Dec1*/*Dec2* were down-regulated (Table 6). Because expression

TABLE 5

Centralized nuclei are enriched exclusively within type I myosin heavy chain-expressing myofibers

ND, not determined.

Name	Central nuclei	Type I+ MHC cells	Type IIA+ MHC cells	Type IIB+ MHC cells	Type X+ MHC cells
	%	%	%	%	%
cKO soleus	14.7 (type I+ cells), 700% increase; 3.4 (type IIA+ cells)	39.85 ± 8.28 ($n = 3$)	60.15 ± 8.28 ($n = 3$)	0	ND
Control soleus	2.1 (type I+ cells); 1.1 (type IIA+ cells)	41.77 ± 9.91 ($n = 3$)	54.52 ± 10.02 ($n = 3$)	3.8	ND
Statistics	$p = 0.000117$	$p = 0.405$	$p = 0.247$		
cKO EDL	0 (type IIA+ cells); 0 (type IIB+ cells)	ND	16.56	68.62	14.61
Control EDL	0 (type IIA+ cells); 0 (type IIB+ cells)	ND	13.61	64.63	21.8

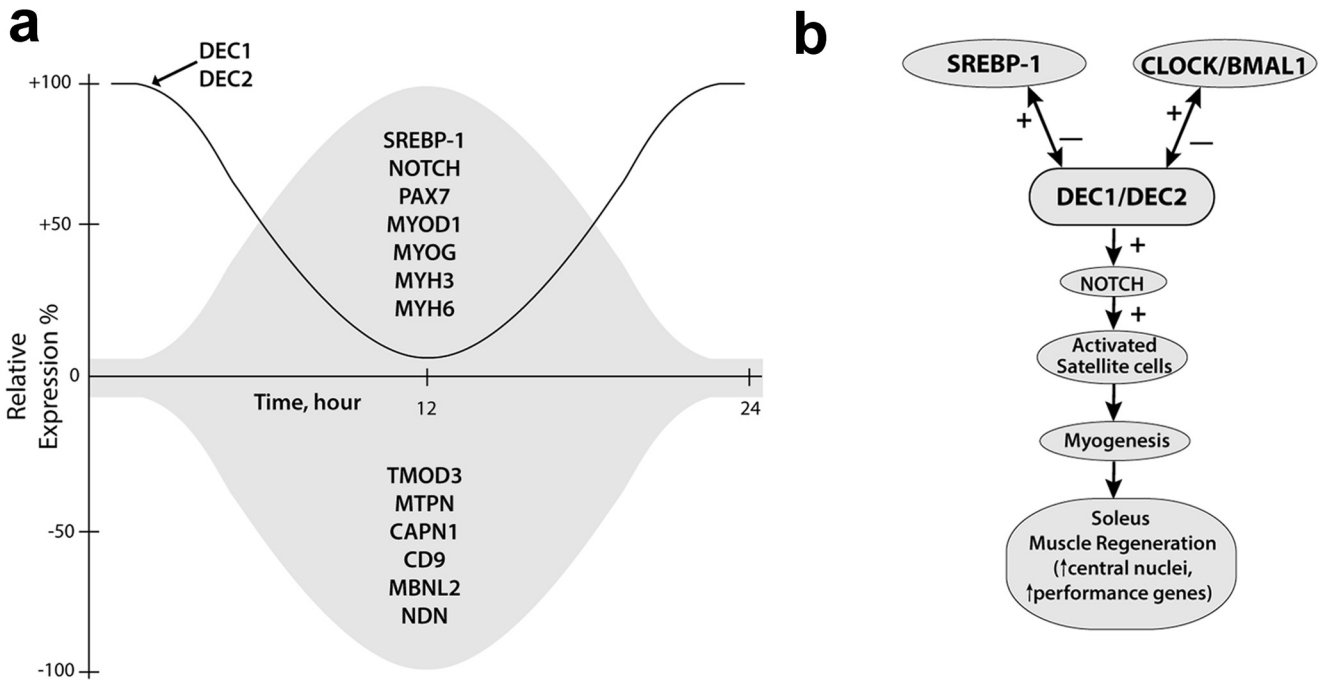

FIGURE 8. **Proposed role of circadian core proteins and transcriptional regulators DEC1/DEC2 in facilitating muscle regeneration by targeting a myogenic pathway in *Dmp1-cre Mbtps1* cKO soleus muscle.** *a*, predicted relative temporal expression patterns in soleus muscle for *Dec1*/*Dec2* in relation to that for a number of myogenic genes (*Srebp1*, *Pax7*, etc.). (Muscle-specific target genes of BHLHE40 and BHLHE41 expressed by *Mbtps1* cKO SOL are listed in Table 6.) *b*, diagram illustrating the complex inter-relationships and feedback loops that interconnect transcriptional regulators DEC1/DEC2 with circadian core clock genes (*Clock*/*Bmal*), MBTPS1-activated transcription factor SREBP1, and NOTCH activation of muscle satellite cells (see "Discussion" for references).

of both *Dec1* and *Dec2* is low in *Dmp1-cre Mbtps1* cKO SOL (array data deposited at NCBI under accession number GSE69985), this is the expected outcome. Although our transcriptional data represent a single time point and not a systematic timed study of circadian regulation, we believe the high degree of correlation between predicted and observed target gene expression observed in Table 6 supports an indirect role for *Dec1*/*Dec2* in the regeneration and growth of *Dmp1-cre Mbtps1* cKO SOL (Table 6 and Fig. 8). Specifically, we propose that bone-muscle cross-talk facilitates circadian cycling of expression of promyogenic genes (including *Pax7*, *Myod1*, and *Myog*) sufficient to form new myofibers from muscle progenitor cells (Table 6 and Fig. 8, *a* and *b*). PAX7 is required for specification of satellite cells from muscle-derived stem cells (47). MYOD1, in turn, generates myogenic precursor cells, which are induced to terminally differentiate to myotubes by MYOG (48). We envision that cyclical waves of expression of these promyogenic genes drives progression of satellite cells through the different stages of muscle specification and differentiation while accommodating for the known cross-inhibitory interactions of individual factors (47, 70).

Gene profiling identified several other signaling pathways that are more highly expressed in *Mbtps1* cKO SOL: EGF receptor signaling, striated muscle contraction, circadian exercise, fatty acid β-oxidation, glycolysis, and adipogenesis. We hypothesize that these pathways reflect major metabolic adaptations, *e.g.* an EGF receptor pathway regulating myoblast differentiation (71), a pathway improving contractile force, and a pathway enhancing oxidative catabolism of fat and sugar nutrients. Increased expression by *Mbtps1* cKO SOL of a number of genes can be rationalized in terms of improving contractile performance. For example, expression of actinin3, titin, and desmin is increased compared with controls. Z-disc component actinin3 is strongly associated with improvements in sprint or endurance (72, 73), whereas titin is also localized to the Z-disc, which mechanically couples sarcomeric contraction and stretching (74, 75). Desmin is required for the tensile strength and integrity of myofibrils (76). Remarkably, *Mg29* is also overexpressed in cKO SOL. Mg29 (also known as synaptophysin-like 2) is essential for proper excitation-contraction coupling in skeletal muscle because null mice have reduced muscle performance due to failures in excitation-contraction

TABLE 6

***Dmp1-cre Mbtps1* cKO soleus muscles express alterations in 79 out of 110 muscle-specific DEC1/DEC2 target genes identified by Lecomte *et al.* (66) that are consistent with a release from transcriptional regulation**

Soleus muscles from *Dmp1-cre Mbtps1* cKO and control mice were isolated and processed for whole genome arrays as described under "Experimental Procedures" (deposited at NCBI under accession number GSE69985). Genes exhibiting significant differences in expression were then compared with the list of muscle-specific DEC1/DEC2 target genes identified by Lecomte *et al.* (66).

Gene symbol	Genes repressed by DEC1/DEC2[a] which are increased in cKO	Genes activated by DEC1/DEC2[b] which are reduced in cKO	Gene symbol	Genes repressed by DEC1/DEC2[a] which are increased in cKO	Genes activated by DEC1/DEC2[b] which are reduced in cKO
ACTA1	+		MTPN		+
ACTN2	+		MYBPH	+	
ACTN3	+		MYH2	+	
AK1	+		MYH3	+	
APOBEC2	+		MYH6	+	
ALS2		+	MYH7	+	
ALS2CR12		+	MYL1	+	
ANKRD2	+		MYL2	+	
AOX1		+	MYOD1	+	
ATP2A1	+		MYOG	+	
ASPH		+	MYOM2	+	
CACNA1S	+		MYPN	+	
CACNB1	+		NDN		+
CACNG1	+		PANK4	+	
CAPN1		+	PAX7	+	
CAV3	+		PFKM	+	
CD9		+	PGAM2	+	
CDH15	+		POPDC2	+	
CDON	+		POPDC3	+	
CFL1	+		PPARGC1A	+	
CHRNA1	+		PRKAG3	+	
CHRNG	+		SEPW1	+	
CKB	+		SGCD	+	
CKM	+		SGCG	+	
CRYAB	+		SLC6A8	+	
DES	+		SNTB1	+	
DMPK	+		SVIL	+	
DNTA		+	SYNE1		+
DYSF	+		TCAP	+	
EEF1A2	+		TMOD3		+
ENO3	+		TNNC1	+	
FKBP1B		+	TNNI1	+	
FLNC	+		TNNT2	+	
FOXO1	+		TRIM54	+	
GNA11		+	TRIM55	+	
GYS1	+		TTN	+	
HDAC4	+		UNC93B1	+	
ITGA7	+		MBNL2		+
KBTBD10		+	MAPK12	+	
LDHA	+				

[a] Expression of genes in this column, which are repressed by BHLHB2/BHLHB3, were increased in soleus muscles from *Dmp1-cre Mbtps1* cKO mice compared with littermate control muscles.

[b] Expression of genes in this column, which are activated by BHLHB2/BHLHB3, were decreased in soleus muscles from *Dmp1-cre Mbtps1* cKO mice compared with littermate control muscles.

coupling, a finding that is also mirrored in aged skeletal muscles, which have an ~50% reduction in the protein content of MG29 (77, 78). In contrast, improved muscle performance in an animal model where the MG29 level was up-regulated has been reported (79). Therefore, the up-regulation of *Mg29* along with the up-regulation of other muscle performance genes helps explain the increased contractile performance of SOL muscles from cKO mice. Consistent with their renewal of type I-expressing myofibers, cKO SOLs also have increased expression of key enzymes that mediate oxidative metabolism of fats and sugars, *e.g.* adipose triglyceride lipase, adiponectin, phosphoenolpyruvate carboxykinase, and phosphofructokinase.

In summary, male *Dmp1-cre Mbtps1* cKO mice display an age-dependent slow twitch muscle phenotype with increased specific contractile force and size. All available evidence supports bone-muscle cross-talk as the cause. Furthermore, gene expression changes in cKO soleus muscles appear entirely consistent with the observed structural and functional changes. Better understanding of bone-muscle cross-talk may provide a fresh and novel approach for the prevention and treatment of age-related muscle loss.

Author Contributions—J. P. G. was the principal investigator, designed and conducted experiments, acquired and analyzed data, wrote the manuscript, provided funding, and following submission carried out additional experiments and revised the manuscript for resubmission. N. T. H. conducted experiments and acquired and analyzed data. J. V. conducted experiments and acquired and analyzed data. L. B. conducted experiments. S. V. C. conducted experiments and acquired and analyzed data. A. B. acquired and analyzed data. A. S. analyzed data. J. H. acquired data. C. M. acquired data. N. G. S. consulted in design of experiments and provided reagents. L. B. consulted in design of experiments, provided partial funding, and contributed to writing the manuscript. M. B. designed experiments, analyzed data, contributed to writing the manuscript, and provided partial funding.

References

1. Dallas, S. L., Prideaux, M., and Bonewald, L. F. (2013) The osteocyte: an endocrine cell and more. *Endocr. Rev.* **34,** 658–690
2. Xiao, Z., Huang, J., Cao, L., Liang, Y., Han, X., and Quarles, L. D. (2014) Osteocyte-specific deletion of Fgfr1 suppresses FGF23. *PLoS One* **9,** e104154
3. Mo, C., Romero-Suarez, S., Bonewald, L., Johnson, M., and Brotto, M.

(2012) Prostaglandin E2: from clinical applications to its potential role in bone-muscle crosstalk and myogenic differentiation. *Recent Pat. Biotechnol.* **6,** 223–229
4. Brotto, M., and Johnson, M. L. (2014) Endocrine crosstalk between muscle and bone. *Curr. Osteoporos. Rep.* **12,** 135–141
5. Shen, H., Grimston, S., Civitelli, R., and Thomopoulos, S. (2015) Deletion of connexin43 in osteoblasts/osteocytes leads to impaired muscle formation in mice. *J. Bone Miner. Res.* **30,** 596–605
6. Jähn, K., Lara-Castillo, N., Brotto, L., Mo, C. L., Johnson, M. L., Brotto, M., and Bonewald, L. F. (2012) Skeletal muscle secreted factors prevent glucocorticoid-induced osteocyte apoptosis through activation of β-catenin. *Eur. Cell. Mater.* **24,** 197–209; discussion 209–110
7. Ciciliot, S., and Schiaffino, S. (2010) Regeneration of mammalian skeletal muscle. Basic mechanisms and clinical implications. *Curr. Pharm. Des.* **16,** 906–914
8. Yin, H., Price, F., and Rudnicki, M. A. (2013) Satellite cells and the muscle stem cell niche. *Physiol. Rev.* **93,** 23–67
9. Kalhovde, J. M., Jerkovic, R., Sefland, I., Cordonnier, C., Calabria, E., Schiaffino, S., and Lømo, T. (2005) "Fast" and "slow" muscle fibres in hindlimb muscles of adult rats regenerate from intrinsically different satellite cells. *J. Physiol.* **562,** 847–857
10. Lagord, C., Soulet, L., Bonavaud, S., Bassaglia, Y., Rey, C., Barlovatz-Meimon, G., Gautron, J., and Martelly, I. (1998) Differential myogenicity of satellite cells isolated from extensor digitorum longus (EDL) and soleus rat muscles revealed *in vitro*. *Cell Tissue Res.* **291,** 455–468
11. Seidah, N. G., Sadr, M. S., Chrétien, M., and Mbikay, M. (2013) The multifaceted proprotein convertases: their unique, redundant, complementary, and opposite functions. *J. Biol. Chem.* **288,** 21473–21481
12. Seidah, N. G., and Prat, A. (2012) The biology and therapeutic targeting of the proprotein convertases. *Nat. Rev. Drug Discov.* **11,** 367–383
13. Gorski, J. P., Huffman, N. T., Chittur, S., Midura, R. J., Black, C., Oxford, J., and Seidah, N. G. (2011) Inhibition of proprotein convertase SKI-1 blocks transcription of key extracellular matrix genes regulating osteoblastic mineralization. *J. Biol. Chem.* **286,** 1836–1849
14. Seidah, N. G., Mayer, G., Zaid, A., Rousselet, E., Nassoury, N., Poirier, S., Essalmani, R., and Prat, A. (2008) The activation and physiological functions of the proprotein convertases. *Int. J. Biochem. Cell Biol.* **40,** 1111–1125
15. Lu, Y., Xie, Y., Zhang, S., Dusevich, V., Bonewald, L. F., and Feng, J. Q. (2007) DMP1-targeted Cre expression in odontoblasts and osteocytes. *J. Dent. Res.* **86,** 320–325
16. Liu, F., Woitge, H. W., Braut, A., Kronenberg, M. S., Lichtler, A. C., Mina, M., and Kream, B. E. (2004) Expression and activity of osteoblast-targeted Cre recombinase transgenes in murine skeletal tissues. *Int. J. Dev. Biol.* **48,** 645–653
17. Achilleos, A., Huffman, N. T., Marcinkiewicyz, E., Seidah, N. G., Chen, Q., Dallas, S. L., Trainor, P. A., and Gorski, J. P. (2015) MBTPS1/SKI-1/S1P proprotein convertase is required for ECM signaling and axial elongation during somitogenesis and vertebral development. *Hum. Mol. Genet.* **24,** 2884–2898
18. Yang, J., Goldstein, J. L., Hammer, R. E., Moon, Y. A., Brown, M. S., and Horton, J. D. (2001) Decreased lipid synthesis in livers of mice with disrupted Site-1 protease gene. *Proc. Natl. Acad. Sci. U.S.A.* **98,** 13607–13612
19. Patra, D., Xing, X., Davies, S., Bryan, J., Franz, C., Hunziker, E. B., and Sandell, L. J. (2007) Site-1 protease is essential for endochondral bone formation in mice. *J. Cell Biol.* **179,** 687–700
20. Clapcote, S. J., and Roder, J. C. (2005) Simplex PCR assay for sex determination in mice. *BioTechniques* **38,** 702, 704, 706
21. Pullikotil, P., Benjannet, S., Mayne, J., and Seidah, N. G. (2007) The proprotein convertase SKI-1/S1P: alternate translation and subcellular localization. *J. Biol. Chem.* **282,** 27402–27413
22. Phillips, C. L., Yamakawa, K., and Adelstein, R. S. (1995) Cloning of the cDNA encoding human nonmuscle myosin heavy chain-B and analysis of human tissues with isoform-specific antibodies. *J. Muscle Res. Cell Motil.* **16,** 379–389
23. Schneider, C. A., Rasband, W. S., and Eliceiri, K. W. (2012) NIH Image to ImageJ: 25 years of image analysis. *Nat. Methods* **9,** 671–675
24. Doube, M., Kłosowski, M. M., Arganda-Carreras, I., Cordelières, F. P., Dougherty, R. P., Jackson, J. S., Schmid, B., Hutchinson, J. R., and Shefelbine, S. J. (2010) BoneJ: free and extensible bone image analysis in ImageJ. *Bone* **47,** 1076–1079
25. Park, K. H., Brotto, L., Lehoang, O., Brotto, M., Ma, J., and Zhao, X. (2012) *Ex vivo* assessment of contractility, fatigability and alternans in isolated skeletal muscles. *J. Vis. Exp.* e4198
26. Thornton, A. M., Zhao, X., Weisleder, N., Brotto, L. S., Bougoin, S., Nosek, T. M., Reid, M., Hardin, B., Pan, Z., Ma, J., Parness, J., and Brotto, M. (2011) Store-operated Ca^{2+} entry (SOCE) contributes to normal skeletal muscle contractility in young but not in aged skeletal muscle. *Aging* **3,** 621–634
27. Shen, J., Yu, W. M., Brotto, M., Scherman, J. A., Guo, C., Stoddard, C., Nosek, T. M., Valdivia, H. H., and Qu, C. K. (2009) Deficiency of MIP/MTMR14 phosphatase induces a muscle disorder by disrupting Ca^{2+} homeostasis. *Nat. Cell Biol.* **11,** 769–776
28. Cai, C., Masumiya, H., Weisleder, N., Matsuda, N., Nishi, M., Hwang, M., Ko, J. K., Lin, P., Thornton, A., Zhao, X., Pan, Z., Komazaki, S., Brotto, M., Takeshima, H., and Ma, J. (2009) MG53 nucleates assembly of cell membrane repair machinery. *Nat. Cell Biol.* **11,** 56–64
29. Huffman, N. T., Keightley, J. A., Chaoying, C., Midura, R. J., Lovitch, D., Veno, P. A., Dallas, S. L., and Gorski, J. P. (2007) Association of specific proteolytic processing of bone sialoprotein and bone acidic glycoprotein-75 with mineralization within biomineralization foci. *J. Biol. Chem.* **282,** 26002–26013
30. Seidah, N. G., Mowla, S. J., Hamelin, J., Mamarbachi, A. M., Benjannet, S., Touré, B. B., Basak, A., Munzer, J. S., Marcinkiewicz, J., Zhong, M., Barale, J. C., Lazure, C., Murphy, R. A., Chrétien, M., and Marcinkiewicz, M. (1999) Mammalian subtilisin/kexin isozyme SKI-1: a widely expressed proprotein convertase with a unique cleavage specificity and cellular localization. *Proc. Natl. Acad. Sci. U.S.A.* **96,** 1321–1326
31. Moore, B. J., Feldman, H. A., and Reid, M. B. (1993) Developmental changes in diaphragm contractile properties. *J. Appl. Physiol.* **75,** 522–526
32. Schmalbruch, H. (1976) The morphology of regeneration of skeletal muscles in the rat. *Tissue Cell* **8,** 673–692
33. Appell, H. J., Forsberg, S., and Hollmann, W. (1988) Satellite cell activation in human skeletal muscle after training: evidence for muscle fiber neoformation. *Int. J. Sports Med.* **9,** 297–299
34. Warhol, M. J., Siegel, A. J., Evans, W. J., and Silverman, L. M. (1985) Skeletal muscle injury and repair in marathon runners after competition. *Am. J. Pathol.* **118,** 331–339
35. Newlands, S., Levitt, L. K., Robinson, C. S., Karpf, A. B., Hodgson, V. R., Wade, R. P., and Hardeman, E. C. (1998) Transcription occurs in pulses in muscle fibers. *Genes Dev.* **12,** 2748–2758
36. Li, Y., and Thompson, W. J. (2011) Nerve terminal growth remodels neuromuscular synapses in mice following regeneration of the postsynaptic muscle fiber. *J. Neurosci.* **31,** 13191–13203
37. Deb, C., Li, B., Baylink, D. J., Xing, W., Zhang, W., Chen, M., Wergedal, J. E., Mohan, S., and Qin, X. (2012) Transgenic overexpression of pregnancy-associated plasma protein-A in skeletal muscle of mice increases myofiber size and central nucleation in sedentary muscle and promotes muscle regeneration in the injured muscle. *Growth Horm. IGF Res.* **22,** 173–179
38. Galbiati, F., Volonte, D., Chu, J. B., Li, M., Fine, S. W., Fu, M., Bermudez, J., Pedemonte, M., Weidenheim, K. M., Pestell, R. G., Minetti, C., and Lisanti, M. P. (2000) Transgenic overexpression of caveolin-3 in skeletal muscle fibers induces a Duchenne-like muscular dystrophy phenotype. *Proc. Natl. Acad. Sci. U.S.A.* **97,** 9689–9694
39. Asmussen, G., Schmalbruch, I., Soukup, T., and Pette, D. (2003) Contractile properties, fiber types, and myosin isoforms in fast and slow muscles of hyperactive Japanese waltzing mice. *Exp. Neurol.* **184,** 758–766
40. Matsuura, T., Li, Y., Giacobino, J. P., Fu, F. H., and Huard, J. (2007) Skeletal muscle fiber type conversion during the repair of mouse soleus: potential implications for muscle healing after injury. *J. Orthop. Res.* **25,** 1534–1540
41. Yang, N., Garton, F., and North, K. (2009) α-Actinin-3 and performance. *Med. Sport Sci.* **54,** 88–101
42. Sartore, S., Gorza, L., and Schiaffino, S. (1982) Fetal myosin heavy chains in regenerating muscle. *Nature* **298,** 294–296
43. Weiss, A., Schiaffino, S., and Leinwand, L. A. (1999) Comparative sequence analysis of the complete human sarcomeric myosin heavy chain family: implications for functional diversity. *J. Mol. Biol.* **290,** 61–75

44. Mathes, A. L., and Lafyatis, R. (2011) Role for Toll-like receptor 3 in muscle regeneration after cardiotoxin injury. *Muscle Nerve* **43,** 733–740
45. Goetsch, S. C., Hawke, T. J., Gallardo, T. D., Richardson, J. A., and Garry, D. J. (2003) Transcriptional profiling and regulation of the extracellular matrix during muscle regeneration. *Physiol. Genomics* **14,** 261–271
46. Rudnicki, M. A., Le Grand, F., McKinnell, I., and Kuang, S. (2008) The molecular regulation of muscle stem cell function. *Cold Spring Harb. Symp. Quant. Biol*. **73,** 323–331
47. Seale, P., Sabourin, L. A., Girgis-Gabardo, A., Mansouri, A., Gruss, P., and Rudnicki, M. A. (2000) Pax7 is required for the specification of myogenic satellite cells. *Cell* **102,** 777–786
48. Olguin, H. C., Yang, Z., Tapscott, S. J., and Olwin, B. B. (2007) Reciprocal inhibition between Pax7 and muscle regulatory factors modulates myogenic cell fate determination. *J. Cell Biol.* **177,** 769–779
49. Reppert, S. M., and Weaver, D. R. (2002) Coordination of circadian timing in mammals. *Nature* **418,** 935–941
50. Coffey, V. G., and Hawley, J. A. (2007) The molecular bases of training adaptation. *Sports Med*. **37,** 737–763
51. Matsuda, R., Spector, D. H., and Strohman, R. C. (1983) Regenerating adult chicken skeletal muscle and satellite cell cultures express embryonic patterns of myosin and tropomyosin isoforms. *Dev. Biol.* **100,** 478–488
52. Grounds, M. D., Garrett, K. L., Lai, M. C., Wright, W. E., and Beilharz, M. W. (1992) Identification of skeletal muscle precursor cells *in vivo* by use of MyoD1 and myogenin probes. *Cell Tissue Res.* **267,** 99–104
53. Blanar, M. A., Crossley, P. H., Peters, K. G., Steingrímsson, E., Copeland, N. G., Jenkins, N. A., Martin, G. R., and Rutter, W. J. (1995) Meso1, a basic-helix-loop-helix protein involved in mammalian presomitic mesoderm development. *Proc. Natl. Acad. Sci. U.S.A.* **92,** 5870–5874
54. Chang, N. C., and Rudnicki, M. A. (2014) Satellite cells: the architects of skeletal muscle. *Curr. Top. Dev. Biol.* **107,** 161–181
55. Mendias, C. L., Marcin, J. E., Calerdon, D. R., and Faulkner, J. A. (2006) Contractile properties of EDL and soleus muscles of myostatin-deficient mice. *J. Appl. Physiol.* **101,** 898–905
56. Amthor, H., Macharia, R., Navarrete, R., Schuelke, M., Brown, S. C., Otto, A., Voit, T., Muntoni, F., Vrbóva, G., Partridge, T., Zammit, P., Bunger, L., and Patel, K. (2007) Lack of myostatin results in excessive muscle growth but impaired force generation. *Proc. Natl. Acad. Sci. U.S.A.* **104,** 1835–1840
57. Personius, K. E., Jayaram, A., Krull, D., Brown, R., Xu, T., Han, B., Burgess, K., Storey, C., Shah, B., Tawil, R., and Welle, S. (2010) Grip force, EDL contractile properties, and voluntary wheel running after postdevelopmental myostatin depletion in mice. *J. Appl. Physiol.* **109,** 886–894
58. Del Prete, Z., Musarò, A., and Rizzuto, E. (2008) Measuring mechanical properties, including isotonic fatigue, of fast and slow MLC/mIgf-1 transgenic skeletal muscle. *Ann. Biomed. Eng.* **36,** 1281–1290
59. Mangner, N., Adams, V., Sandri, M., Hoellriegel, R., Hambrecht, R., Schuler, G., and Gielen, S. (2012) Muscle function and running activity in mouse models of hereditary muscle dystrophy: impact of double knockout for dystrophin and the transcription factor MyoD. *Muscle Nerve* **45,** 544–551
60. Fougerousse, F., Gonin, P., Durand, M., Richard, I., and Raymackers, J. M. (2003) Force impairment in calpain 3-deficient mice is not correlated with mechanical disruption. *Muscle Nerve* **27,** 616–623
61. Honma, S., Kawamoto, T., Takagi, Y., Fujimoto, K., Sato, F., Noshiro, M., Kato, Y., and Honma, K. (2002) Dec1 and Dec2 are regulators of the mammalian molecular clock. *Nature* **419,** 841–844
62. Hamaguchi, H., Fujimoto, K., Kawamoto, T., Noshiro, M., Maemura, K., Takeda, N., Nagai, R., Furukawa, M., Honma, S., Honma, K., Kurihara, H., and Kato, Y. (2004) Expression of the gene for Dec2, a basic helix-loop-helix transcription factor, is regulated by a molecular clock system. *Biochem. J.* **382,** 43–50
63. Kawamoto, T., Noshiro, M., Sato, F., Maemura, K., Takeda, N., Nagai, R., Iwata, T., Fujimoto, K., Furukawa, M., Miyazaki, K., Honma, S., Honma, K. i., and Kato, Y. (2004) A novel autofeedback loop of Dec1 transcription involved in circadian rhythm regulation. *Biochem. Biophys. Res. Commun.* **313,** 117–124
64. Wu, T., Ni, Y., Zhuge, F., and Fu, Z. (2010) Resetting process of peripheral circadian gene expression after the combined reversal of feeding schedule and light/dark cycle via a 24-h light period transition in rats. *Physiol. Res*. **59,** 581–590
65. Chatterjee, S., Yin, H., Nam, D., Li, Y., and Ma, K. (2015) Brain and muscle Arnt-like 1 promotes skeletal muscle regeneration through satellite cell expansion. *Exp. Cell Res.* **331,** 200–210
66. Lecomte, V., Meugnier, E., Euthine, V., Durand, C., Freyssenet, D., Nemoz, G., Rome, S., Vidal, H., and Lefai, E. (2010) A new role for sterol regulatory element binding protein 1 transcription factors in the regulation of muscle mass and muscle cell differentiation. *Mol. Cell. Biol.* **30,** 1182–1198
67. Rome, S., Lecomte, V., Meugnier, E., Rieusset, J., Debard, C., Euthine, V., Vidal, H., and Lefai, E. (2008) Microarray analyses of SREBP-1a and SREBP-1c target genes identify new regulatory pathways in muscle. *Physiol. Genomics* **34,** 327–337
68. Acharjee, S., Chung, T. K., Gopinadhan, S., Shankar, S. R., Wang, Y., Li, L., Vercherat, C., Gulbagci, N. T., Rossner, M., and Taneja, R. (2014) Sharp-1 regulates TGF-β signaling and skeletal muscle regeneration. *J. Cell Sci.* **127,** 599–608
69. Sun, H., Li, L., Vercherat, C., Gulbagci, N. T., Acharjee, S., Li, J., Chung, T. K., Thin, T. H., and Taneja, R. (2007) Stra13 regulates satellite cell activation by antagonizing Notch signaling. *J. Cell Biol.* **177,** 647–657
70. Dey, B. K., Gagan, J., and Dutta, A. (2011) miR-206 and -486 induce myoblast differentiation by downregulating Pax7. *Mol. Cell. Biol.* **31,** 203–214
71. Leroy, M. C., Perroud, J., Darbellay, B., Bernheim, L., and Konig, S. (2013) Epidermal growth factor receptor down-regulation triggers human myoblast differentiation. *PLoS One* **8,** e71770
72. MacArthur, D. G., Seto, J. T., Chan, S., Quinlan, K. G., Raftery, J. M., Turner, N., Nicholson, M. D., Kee, A. J., Hardeman, E. C., Gunning, P. W., Cooney, G. J., Head, S. I., Yang, N., and North, K. N. (2008) An Actn3 knockout mouse provides mechanistic insights into the association between α-actinin-3 deficiency and human athletic performance. *Hum. Mol. Genet.* **17,** 1076–1086
73. Norman, B., Esbjörnsson, M., Rundqvist, H., Österlund, T., Glenmark, B., and Jansson, E. (2014) ACTN3 genotype and modulation of skeletal muscle response to exercise in human subjects. *J. Appl. Physiol.* **116,** 1197–1203
74. Rassier, D. E., Lee, E. J., and Herzog, W. (2005) Modulation of passive force in single skeletal muscle fibres. *Biol. Lett.* **1,** 342–345
75. Herzog, W. (2014) The role of titin in eccentric muscle contraction. *J. Exp. Biol.* **217,** 2825–2833
76. Li, Z., Mericskay, M., Agbulut, O., Butler-Browne, G., Carlsson, L., Thornell, L. E., Babinet, C., and Paulin, D. (1997) Desmin is essential for the tensile strength and integrity of myofibrils but not for myogenic commitment, differentiation, and fusion of skeletal muscle. *J. Cell Biol.* **139,** 129–144
77. Brotto, M. A., Nagaraj, R. Y., Brotto, L. S., Takeshima, H., Ma, J. J., and Nosek, T. M. (2004) Defective maintenance of intracellular Ca^{2+} homeostasis is linked to increased muscle fatigability in the MG29 null mice. *Cell Res*. **14,** 373–378
78. Weisleder, N., Brotto, M., Komazaki, S., Pan, Z., Zhao, X., Nosek, T., Parness, J., Takeshima, H., and Ma, J. (2006) Muscle aging is associated with compromised Ca^{2+} spark signaling and segregated intracellular Ca^{2+} release. *J. Cell Biol.* **174,** 639–645
79. Zhao, X., Yoshida, M., Brotto, L., Takeshima, H., Weisleder, N., Hirata, Y., Nosek, T. M., Ma, J., and Brotto, M. (2005) Enhanced resistance to fatigue and altered calcium handling properties of sarcalumenin knockout mice. *Physiol. Genomics* **23,** 72–78